

Breaking the Dimensional Barrier: A Pontryagin-Guided Direct Policy Optimization for Continuous-Time Multi-Asset Portfolio

Jeonggyu Huh¹, Jaegi Jeon^{*2}, and Hyeng Keun Koo³

¹Department of Mathematics, Sungkyunkwan University, Republic of Korea

²Graduate School of Data Science, Chonnam National University, Republic of Korea

³Department of Financial Engineering, Ajou University, Republic of Korea

April 16, 2025

Abstract

Solving large-scale, continuous-time portfolio optimization problems involving numerous assets and state-dependent dynamics has long been challenged by the curse of dimensionality. Traditional dynamic programming and PDE-based methods, while rigorous, typically become computationally intractable beyond a small number of state variables (often limited to 3-6 in prior numerical studies). To overcome this critical barrier, we introduce the *Pontryagin-Guided Direct Policy Optimization* (PG-DPO) framework. PG-DPO leverages Pontryagin’s Maximum Principle to directly guide neural network policies via backpropagation-through-time, naturally incorporating exogenous state processes without requiring dense state grids. Crucially, our computationally efficient “Two-Stage” variant exploits rapidly stabilizing costate estimates derived from BPTT, converting them into near-optimal closed-form Pontryagin controls after only a short warm-up, significantly reducing training overhead. This enables a breakthrough in scalability: numerical experiments demonstrate that PG-DPO successfully tackles problems with dimensions previously considered far out of reach, optimizing portfolios with up to 50 assets and 10 state variables. The framework delivers near-optimal policies, offering a practical and powerful alternative for high-dimensional continuous-time portfolio choice.

*Corresponding Author: jaegijeon@jnu.ac.kr

1 Introduction

High-dimensional optimal control problems often fall prey to the “curse of dimensionality” (Bellman, 1966), whereby the computational cost of classical dynamic programming (DP) approaches grows exponentially with the number of state variables. In a continuous-time finance setting, this difficulty becomes starkly evident in multi-asset Merton problems (Merton, 1971), where an investor dynamically allocates wealth among numerous risky assets whose drift and volatility may depend on exogenous state variables such as macroeconomic indicators or stochastic volatility factors. While DP or Hamilton–Jacobi–Bellman (HJB) PDE solvers provide a rigorous framework for low-dimensional cases (Bertsekas & Tsitsiklis, 1995), they become intractable as the number of assets or state dimensions increases, with prior influential studies often limited to analyzing problems involving up to approximately 3-5 state variables (Campbell & Viceira, 1999; Lynch, 2001; Balduzzi & Lynch, 1999) or specific frameworks handling around 6 state variables (Garlappi & Skoulakis, 2010), often necessitating simulation-based approaches for tractability (Brandt et al., 2005).

A promising alternative is to employ *Pontryagin’s Maximum Principle (PMP)*, an indirect method that bypasses the explicit computation of value functions (Pontryagin, 2014; Yong & Zhou, 2012). Rather than storing or approximating a high-dimensional value grid, the PMP characterizes the optimal control in terms of forward–backward differential equations for the state and its *costate* (adjoint). Notably, adding one more state dimension does not produce an exponential explosion in computational requirements, in contrast to DP (Bellman, 1966; Campbell et al., 2003). This makes Pontryagin-based methods appealing for large-scale portfolio optimization problems involving many assets and exogenous state processes (Karatzas et al., 1987).

Recent advances in deep learning further enhance the scalability of methods for solving high-dimensional stochastic control problems (e.g., Han et al., 2018; Raissi et al., 2019, for general PDE-based approaches). Concurrently, deep learning techniques are being applied directly to financial dynamic programming. Some approaches tackle infinite horizon problems via the HJB equation (Duarte et al., 2024), while others aim to directly solve the associated nonlinear PDEs using methods like deep branching algorithms (Nguwi et al., 2024). However, applications such as the Merton HJB have revealed limitations in accuracy or efficiency for certain PDE solvers like Deep BSDE variants (Nguwi et al., 2024). Our approach, distinct from these direct HJB/PDE solvers, focuses on using Pontryagin’s principle, readily handling finite horizons. One notable strategy related to the use of adjoint methods in optimal control is to *directly* parameterize the policy (i.e., consumption and investment controls) with neural networks, then apply backpropagation-through-time (BPTT) to enforce Pontryagin’s optimality condi-

tions (Huh, 2024). This strategy, known as “Pontryagin-Guided Direct Policy Optimization (PG-DPO),” circumvents the need to approximate value functions or PDE solutions. Instead, it uses simulation-based gradients that automatically incorporate the adjoint processes, drastically reducing computational overhead in high-dimensional settings (Kushner & Yin, 2003; Borkar & Borkar, 2008).

The purpose of this paper is to develop and implement this PG-DPO framework for the general *multi-asset, state-dependent* continuous-time portfolio problem. We consider an investor who must decide on a continuous consumption rate and an allocation to n risky assets with state-dependent drift and volatility. By parameterizing the policy with neural networks, we can capture potentially complex relationships dependent on both wealth and the exogenous state. We show how a single forward pass in simulation, coupled with a backward pass via automatic differentiation (BPTT), yields unbiased estimates of the costate processes that PMP requires, guiding the policy towards optimality without the drawbacks of DP.

Furthermore, we introduce a “Two-Stage” PG-DPO variant that exploits the observation that costate estimates often stabilize much faster than the full policy network. Once the costates are sufficiently stable (after a short warm-up), one can *bypass* the potentially suboptimal neural policy outputs and directly substitute the costate estimates into the PMP first-order conditions. This recovers a near-optimal control analytically at every time-state point with minimal additional training, significantly reducing computational burden while maintaining high accuracy. This efficiency enables the solution of problems with **dozens of assets and state variables (e.g., $n=50$, $k=10$ in our experiments)**, a scale considerably larger than those typically addressed by the numerical methods cited previously.

The main contributions of this paper can be summarized as follows:

- We develop and implement the Pontryagin-Guided Direct Policy Optimization (PG-DPO) framework, leveraging PMP and deep learning, for solving general multi-asset, multi-factor continuous-time portfolio optimization problems with state-dependent dynamics and finite horizons.
- We introduce a computationally efficient “Two-Stage” PG-DPO variant that utilizes rapidly stabilized costate estimates from BPTT directly within the PMP first-order conditions, significantly reducing training overhead while achieving high accuracy.
- We demonstrate through numerical experiments that our framework, particularly the Two-Stage variant, successfully scales to high-dimensional problems involving dozens of assets and state variables (up to $n=50$, $k=10$). This substantially exceeds the dimensionality manageable by traditional DP

methods and tackled in many prior numerical studies focusing on problems with typically fewer than 5-6 state variables, thus effectively mitigating the curse of dimensionality.

In the remainder of this paper, we first present the multi-asset Merton problem with exogenous states in Section 2. We focus on the affine multi-factor OU model, detailed in Section 2.3.2, for developing the methodology and conducting numerical experiments due to the availability of a benchmark solution. Section 3 introduces our Pontryagin-Guided Direct Policy Optimization (PG-DPO) algorithm and its Two-Stage extension. Numerical experiments presented in Section 4 confirm the framework’s scalability and near-optimal performance for the affine model. Finally, Section 5 concludes and discusses potential future directions, including applications to non-affine models or problems with portfolio constraints.

2 Multi-Asset Continuous-Time Portfolio Problem with State Variables

In this section, we present a multi-asset extension of Merton’s continuous-time portfolio problem (Merton, 1971), allowing the investor to allocate wealth across multiple (potentially correlated) risky assets and a risk-free asset, while consuming continuously. Each risky asset features its own drift and volatility, leading to an n -dimensional *portfolio weight* vector $\boldsymbol{\pi}_t$. Furthermore, an exogenous *state process* $\mathbf{Y}_t \in \mathbb{R}^k$ influences market parameters such as returns and interest rates, adding additional complexity to the investor’s decision.

Although the wealth X_t remains scalar, the investor’s optimal policy now depends on both $\boldsymbol{\pi}_t \in \mathbb{R}^n$ and a high-dimensional state \mathbf{Y}_t . We handle this through Pontryagin’s maximum principle (Pontryagin, 2014; Yong & Zhou, 2012), introducing a costate for X_t and another for \mathbf{Y}_t . Numerically, one can represent $\{\boldsymbol{\pi}_t, C_t\}$ via neural networks, thereby enabling policy gradient or dynamic programming algorithms even in multi-asset, state-dependent environments.

2.1 Problem Formulation with State Variables and Neural Network Controls

Let $\mathbf{Y}_t \in \mathbb{R}^k$ be a vector of state variables that affect the distribution of asset returns. For instance, \mathbf{Y}_t can include interest rates, macroeconomic indices, volatility factors, and so forth. We assume each component $Y_{i,t}$ follows an Ito diffusion

$$dY_{i,t} = \mu_{Y,i}(t, \mathbf{Y}_t) dt + \sigma_{Y,i}(t, \mathbf{Y}_t) dW_{i,t}^Y, \quad i = 1, \dots, k,$$

with $\text{Cov}(dW_{i,t}^Y, dW_{j,t}^Y) = \phi_{ij} dt$. In vector form,

$$d\mathbf{Y}_t = \boldsymbol{\mu}_Y(t, \mathbf{Y}_t) dt + \boldsymbol{\sigma}_Y(t, \mathbf{Y}_t) d\mathbf{W}_t^Y,$$

where $\boldsymbol{\mu}_Y(t, \mathbf{Y}_t)$ is the $k \times 1$ drift vector, $\boldsymbol{\sigma}_Y(t, \mathbf{Y}_t)$ is often assumed to be a $k \times k$ diagonal matrix of diffusion coefficients, and \mathbf{W}_t^Y is a $k \times 1$ vector of potentially correlated Brownian motions driving the state variables.

We consider a financial market with n risky assets and one risk-free asset. For $i = 1, \dots, n$, the price $S_{i,t}$ of the i -th risky asset follows

$$dS_{i,t} = S_{i,t}(\mu_i(t, \mathbf{Y}_t) dt + \sigma_i(t, \mathbf{Y}_t) dW_{i,t}^X).$$

Here, $\mu_i(t, \mathbf{Y}_t)$ is the instantaneous expected return and $\sigma_i(t, \mathbf{Y}_t)$ is the instantaneous volatility of asset i . The n scalar Brownian motions $W_{i,t}^X$ may be correlated amongst themselves ($\text{Cov}(dW_{i,t}^X, dW_{j,t}^X) = \psi_{ij} dt$) and with the state variable processes ($\text{Cov}(dW_{i,t}^X, dW_{j,t}^Y) = \rho_{ij} dt$). In vector notation, let $\boldsymbol{\mu}(t, \mathbf{Y}_t)$ be the $n \times 1$ vector of expected returns, $\boldsymbol{\sigma}(t, \mathbf{Y}_t)$ be the $n \times n$ diagonal matrix of volatilities, and \mathbf{W}_t^X be the $n \times 1$ vector of Brownian motions. The risky asset dynamics can be written compactly as

$$d\mathbf{S}_t = \boldsymbol{\mu}(t, \mathbf{Y}_t) \mathbf{S}_t dt + \boldsymbol{\sigma}(t, \mathbf{Y}_t) \mathbf{S}_t d\mathbf{W}_t^X.$$

Let X_t denote the investor's total wealth. At each time t , the investor chooses a *consumption rate* $C_t \geq 0$ and allocates fractions of wealth to the n risky assets, represented by the vector $\boldsymbol{\pi}_t = (\pi_{1,t}, \dots, \pi_{n,t})^\top \in \mathbb{R}^n$. The remaining fraction $1 - \boldsymbol{\pi}_t^\top \mathbf{1}$ is allocated to the risk-free asset, which earns interest at rate $r(t, \mathbf{Y}_t)$. The wealth process then evolves according to the stochastic differential equation (SDE):

$$dX_t = \left[X_t \left((1 - \boldsymbol{\pi}_t^\top \mathbf{1}) r(t, \mathbf{Y}_t) + \boldsymbol{\pi}_t^\top \boldsymbol{\mu}(t, \mathbf{Y}_t) \right) - C_t \right] dt + X_t \boldsymbol{\pi}_t^\top \boldsymbol{\sigma}(t, \mathbf{Y}_t) d\mathbf{W}_t^X.$$

We require the controls $(\boldsymbol{\pi}_t, C_t)$ to be *admissible*, ensuring that the wealth remains strictly positive, $X_t > 0$, for all $t \in [0, T]$. This condition is essential for the utility function to be well-defined and is typically maintained in simulations (e.g., by clamping wealth at a small positive threshold, see Section 4.1.2).

For clarity on the noise structure, we define the combined $(n+k)$ -dimensional Brownian vector $\mathbf{W}_t = (\mathbf{W}_t^{X^\top}, \mathbf{W}_t^{Y^\top})^\top$. The covariance structure of its increments $d\mathbf{W}_t$ is given by the block matrix:

$$\text{Cov}(d\mathbf{W}_t) = \begin{pmatrix} \Psi & \rho \\ \rho^\top & \Phi \end{pmatrix} dt,$$

where $\Psi \in \mathbb{R}^{n \times n} = \text{Cov}(d\mathbf{W}_t^X)/dt$, $\Phi \in \mathbb{R}^{k \times k} = \text{Cov}(d\mathbf{W}_t^Y)/dt$, and $\rho \in \mathbb{R}^{n \times k} = \text{Cov}(d\mathbf{W}_t^X, d\mathbf{W}_t^Y)/dt$.

The investor's objective is to choose admissible control processes $(\boldsymbol{\pi}, C)$ to maximize the expected discounted utility functional J :

$$J(\boldsymbol{\pi}, C) = \mathbb{E}\left[\int_0^T e^{-\delta t} U(C_t) dt + \kappa e^{-\delta T} U(X_T)\right],$$

subject to the wealth dynamics. Here $\delta > 0$ is the subjective discount rate, and $\kappa \geq 0$ weights the utility of terminal wealth (bequest motive). The utility function $U : (0, \infty) \rightarrow \mathbb{R}$ represents the investor's preferences and is assumed to be strictly increasing, strictly concave, and satisfy the Inada conditions. A widely used specification is the Constant Relative Risk Aversion (CRRA) form:

$$U(x) = \begin{cases} \frac{x^{1-\gamma}}{1-\gamma}, & \gamma > 0, \gamma \neq 1, \\ \ln(x), & \gamma = 1, \end{cases}$$

with $\gamma > 0$ denoting the coefficient of relative risk aversion.

In our numerical approach, we parameterize the control policies using neural networks:

$$\boldsymbol{\pi}_t = \boldsymbol{\pi}_\theta(t, X_t, \mathbf{Y}_t), \quad C_t = C_\phi(t, X_t, \mathbf{Y}_t),$$

where θ and ϕ represent the trainable parameters of the respective neural networks.

2.2 Pontryagin's Maximum Principle with a State-Dependent Market and Costate for \mathbf{Y}_t

We now consider the continuous-time portfolio problem from Section 2.1 under a market whose parameters depend on the exogenous state process $\{\mathbf{Y}_t\}_{0 \leq t \leq T}$. The Pontryagin Maximum Principle (PMP) provides necessary conditions for optimality via a system of forward-backward stochastic differential equations (FBSDEs).

The state of the system consists of the investor's wealth X_t and the exogenous state variables $\mathbf{Y}_t \in \mathbb{R}^k$. We introduce the costate processes associated with these states: $\lambda_t \approx \frac{\partial V}{\partial x}(t, X_t, \mathbf{Y}_t)$ (scalar costate for wealth) and $\boldsymbol{\eta}_t \approx \frac{\partial V}{\partial \mathbf{y}}(t, X_t, \mathbf{Y}_t)$ (a k -dimensional costate vector for the state variables), where V is the value function of the problem. The dynamics of the state and costate processes are described by the following FBSDE system.

Under an optimal control policy $(\boldsymbol{\pi}_t^*, C_t^*)$, the state processes (X_t^*, \mathbf{Y}_t^*) evolve according to the forward SDEs:

$$\begin{aligned} dX_t^* &= \left[X_t^* \left((1 - \boldsymbol{\pi}_t^{*\top} \mathbf{1}) r(t, \mathbf{Y}_t^*) + \boldsymbol{\pi}_t^{*\top} \boldsymbol{\mu}(t, \mathbf{Y}_t^*) \right) - C_t^* \right] dt \\ &\quad + X_t^* \boldsymbol{\pi}_t^{*\top} \boldsymbol{\sigma}(t, \mathbf{Y}_t^*) d\mathbf{W}_t^X, \\ d\mathbf{Y}_t^* &= \boldsymbol{\mu}_Y(t, \mathbf{Y}_t^*) dt + \boldsymbol{\sigma}_Y(t, \mathbf{Y}_t^*) d\mathbf{W}_t^Y, \quad X_0^* = x_0 > 0, \quad \mathbf{Y}_0^* = \mathbf{y}_0 \in \mathbb{R}^k. \end{aligned} \tag{1}$$

Here $\boldsymbol{\sigma}(t, \mathbf{Y}_t^*)$ is the $n \times n$ (diagonal) matrix of volatilities, and $\boldsymbol{\sigma}_Y(t, \mathbf{Y}_t^*)$ is the $k \times k$ diffusion matrix for \mathbf{Y}_t^* . The Brownian motions $\mathbf{W}_t^X \in \mathbb{R}^n$ and $\mathbf{W}_t^Y \in \mathbb{R}^k$ have the covariance structure $\text{Cov}(d\mathbf{W}_t) = \begin{pmatrix} \Psi & \rho \\ \rho^\top & \Phi \end{pmatrix} dt$.

Simultaneously, the costate processes $(\lambda_t^*, \boldsymbol{\eta}_t^*)$ satisfy the backward SDEs (BSDEs):

$$-d\lambda_t^* = \mathcal{H}_x(t, X_t^*, \mathbf{Y}_t^*, \boldsymbol{\pi}_t^*, C_t^*, \lambda_t^*, \boldsymbol{\eta}_t^*) dt - \mathbf{Z}_t^{\lambda X} d\mathbf{W}_t^X - \mathbf{Z}_t^{\lambda Y} d\mathbf{W}_t^Y, \quad (2)$$

$$-d\boldsymbol{\eta}_t^* = \mathcal{H}_y(t, X_t^*, \mathbf{Y}_t^*, \boldsymbol{\pi}_t^*, C_t^*, \lambda_t^*, \boldsymbol{\eta}_t^*) dt - \mathbf{Z}_t^{\eta X} d\mathbf{W}_t^X - \mathbf{Z}_t^{\eta Y} d\mathbf{W}_t^Y. \quad (3)$$

Here, \mathcal{H}_x and \mathcal{H}_y denote the partial derivatives of the Hamiltonian function \mathcal{H} with respect to x and \mathbf{y} , evaluated at the optimal state and controls. The terms $\mathbf{Z}_t^{\lambda X}, \mathbf{Z}_t^{\lambda Y}, \mathbf{Z}_t^{\eta X}, \mathbf{Z}_t^{\eta Y}$ are adapted processes representing the diffusion coefficients of the costates, related to second derivatives of the value function and the system's volatility. The terminal conditions are $\lambda_T^* = \kappa e^{-\delta T} U'(X_T^*)$ and $\boldsymbol{\eta}_T^* = \mathbf{0}$.

The Hamiltonian \mathcal{H} associated with this control problem, whose partial derivatives appear in the BSDE drift terms, is given by:

$$\begin{aligned} \mathcal{H}(t, x, \mathbf{y}, \boldsymbol{\pi}, C, \lambda, \boldsymbol{\eta}) = & e^{-\delta t} U(C) + \lambda \left[x((1 - \boldsymbol{\pi}^\top \mathbf{1})r(t, \mathbf{y}) + \boldsymbol{\pi}^\top \boldsymbol{\mu}(t, \mathbf{y})) - C \right] \\ & + \boldsymbol{\eta}^\top \boldsymbol{\mu}_Y(t, \mathbf{y}). \end{aligned}$$

Optimality requires that the controls $(\boldsymbol{\pi}_t^*, C_t^*)$ maximize the Hamiltonian at each time t . The first-order condition (FOC) with respect to consumption C_t yields $e^{-\delta t} U'(C_t^*) - \lambda_t^* = 0$, implying $C_t^* = (U')^{-1}(e^{\delta t} \lambda_t^*)$. The FOC with respect to the portfolio weights $\boldsymbol{\pi}_t$ leads to a condition balancing expected excess returns against risk, involving the costate λ_t^* and its sensitivity $\mathbf{Z}_t^{\lambda X}$. A standard form for this condition is:

$$\lambda_t^* [\boldsymbol{\mu}(t, \mathbf{Y}_t^*) - r(t, \mathbf{Y}_t^*) \mathbf{1}] + \boldsymbol{\sigma}(t, \mathbf{Y}_t^*) \mathbf{Z}_t^{\lambda X, \top} = \mathbf{0}. \quad (4)$$

Here, $\mathbf{Z}_t^{\lambda X}$ is represented as a $1 \times n$ row vector.

Using Ito's lemma to relate $\mathbf{Z}_t^{\lambda X}$ to the value function derivatives ($\lambda_t = V_X(t, X_t, \mathbf{Y}_t)$, so $\partial_x \lambda_t = V_{XX}$, $\partial_Y \lambda_t = V_{XY}$), one can solve the FOC (4) for the optimal portfolio $\boldsymbol{\pi}_t^*$. The resulting expression, consistent with standard results in continuous-time finance, is:

$$\begin{aligned} \boldsymbol{\pi}_t^* = & -\frac{\lambda_t^*}{X_t^* (\partial_x \lambda_t^*)} \Sigma(t, \mathbf{Y}_t^*)^{-1} (\boldsymbol{\mu}(t, \mathbf{Y}_t^*) - r(t, \mathbf{Y}_t^*) \mathbf{1}) \\ & - \frac{1}{X_t^* (\partial_x \lambda_t^*)} \Sigma(t, \mathbf{Y}_t^*)^{-1} \boldsymbol{\sigma}(t, \mathbf{Y}_t^*) \rho \boldsymbol{\sigma}_Y(t, \mathbf{Y}_t^*)^\top (\partial_Y \lambda_t^*)^\top. \end{aligned} \quad (5)$$

Here, $\Sigma(t, \mathbf{Y}_t^*) = \boldsymbol{\sigma}(t, \mathbf{Y}_t^*) \Psi \boldsymbol{\sigma}(t, \mathbf{Y}_t^*)^\top$ is the instantaneous covariance matrix of asset returns (assuming $\boldsymbol{\sigma}$ is diagonal, this matches previous definition). The

first term represents the *myopic demand*, driven by instantaneous expected excess return and risk aversion. The second term represents the *intertemporal hedging demand*, driven by the desire to hedge against unfavorable changes in the state variables \mathbf{Y}_t , depending on the sensitivity of marginal utility to state variables ($\partial_{\mathbf{Y}} \lambda_t^*$), state variable volatility ($\boldsymbol{\sigma}_Y$), and correlations (ρ, Ψ, Φ).

In the special case $n = 1, k = 1$, we have $\Sigma = \sigma^2$, $\Psi = 1$, ρ is a scalar correlation, $\boldsymbol{\sigma} = \sigma$, $\boldsymbol{\sigma}_Y = \sigma_Y$. The formula (5) simplifies to:

$$\pi_t^* = -\frac{1}{X_t^* (\partial_x \lambda_t^*) \sigma^2} \left\{ \lambda_t^* (\mu(t, Y_t^*) - r(t, Y_t^*)) + \sigma \rho \sigma_Y (\partial_Y \lambda_t^*) \right\},$$

which clearly separates the myopic and hedging components.

2.3 Applications to Financial Models

2.3.1 A Multi-Asset Model with One OU Factor

We first consider a model with n risky assets whose risk premia are driven by a single Ornstein–Uhlenbeck (OU) factor. Specifically, each asset i has a constant volatility $\sigma_i > 0$ and a time-varying risk premium proportional to an OU state variable Y_t , such that the expected return is $r + \alpha_i \sigma_i Y_t$, where r is the constant risk-free rate and α_i is a loading coefficient. The state variable Y_t follows the OU process:

$$dY_t = \kappa_Y (\theta_Y - Y_t) dt + \sigma_Y dW_t^Y,$$

where $\kappa_Y > 0$ is the mean-reversion speed, $\theta_Y \in \mathbb{R}$ is the long-term mean, and $\sigma_Y > 0$ is the factor volatility. The Brownian motion W_t^Y may be correlated with the asset return processes.

The price dynamics for the i -th risky asset, $S_{i,t}$, are given by:

$$\frac{dS_{i,t}}{S_{i,t}} = (r + \alpha_i \sigma_i Y_t) dt + \sigma_i dW_{i,t}^S.$$

The Brownian motions driving the assets, $\mathbf{W}_t^S = (W_{1,t}^S, \dots, W_{n,t}^S)^\top$, have an $n \times n$ covariance matrix Ψdt , i.e., $\text{Cov}(d\mathbf{W}_t^S) = \Psi dt$. Furthermore, each $dW_{i,t}^S$ may have a correlation ρ_i with dW_t^Y ; let $\boldsymbol{\rho} = (\rho_1, \dots, \rho_n)^\top$.

Let X_t denote total wealth. The investor chooses a consumption rate $C_t \geq 0$ and portfolio weights $\boldsymbol{\pi}_t \in \mathbb{R}^n$ for the risky assets. The wealth dynamics follow:

$$dX_t = [X_t ((1 - \boldsymbol{\pi}_t^\top \mathbf{1}) r + \boldsymbol{\pi}_t^\top (r \mathbf{1} + \boldsymbol{\alpha} \boldsymbol{\sigma} Y_t)) - C_t] dt + X_t \boldsymbol{\pi}_t^\top \text{diag}(\boldsymbol{\sigma}) d\mathbf{W}_t^S,$$

where $\boldsymbol{\alpha} = (\alpha_1, \dots, \alpha_n)^\top$, and $\boldsymbol{\sigma} = (\sigma_1, \dots, \sigma_n)^\top$. The instantaneous covariance matrix of the n -asset returns is $\Sigma = \text{diag}(\boldsymbol{\sigma}) \Psi \text{diag}(\boldsymbol{\sigma})$.

For an investor with CRRA utility $U(x)$ and discount rate $\delta > 0$, the optimal consumption C_t^* is determined by $C_t^* = (U')^{-1}(e^{\delta t} \lambda_t^*)$, where λ_t^* is the costate associated with wealth X_t . The PMP first-order condition yields the optimal portfolio $\boldsymbol{\pi}_t^* \in \mathbb{R}^n$ as:

$$\boldsymbol{\pi}_t^* = -\frac{1}{X_t^* (\partial_x \lambda_t^*)} \Sigma^{-1} \{ \lambda_t^* (\boldsymbol{\alpha} \boldsymbol{\sigma}) Y_t + (\partial_Y \lambda_t^*) \sigma_Y (\boldsymbol{\sigma} \boldsymbol{\rho}) \}.$$

This expression involves the costate λ_t^* and its derivatives $\partial_x \lambda_t^*$ and $\partial_Y \lambda_t^*$. The first term within the braces represents the myopic demand driven by the risk premium $(\boldsymbol{\alpha} \boldsymbol{\sigma}) Y_t$, and the second term captures the intertemporal hedging demand arising from the state variable Y_t . If $n = 1$, this simplifies to $\pi_t^* = -\frac{1}{\sigma^2 X_t^* \partial_x \lambda_t^*} \{ \lambda_t^* \alpha \sigma Y_t + \sigma (\partial_Y \lambda_t^*) \sigma_Y \rho \}$. For the specific case without intermediate consumption ($C_t = 0$), an analytic solution involving Riccati ODEs can be derived using the HJB framework (Kim & Omberg, 1996), as detailed in Appendix B.1.

2.3.2 A Multi-Asset, Multi-Factor Model

We then extend this setup to a more general *multi-factor* environment, considering n risky assets whose risk premia are driven by a k -dimensional OU factor vector $\mathbf{Y}_t \in \mathbb{R}^k$. The risk premium for asset $i = 1, \dots, n$ is $\sigma_i (\boldsymbol{\alpha}_i^\top \mathbf{Y}_t)$, where $\boldsymbol{\alpha}_i \in \mathbb{R}^k$ contains the factor loadings for asset i . The volatility σ_i for asset i is constant. This allows for richer interactions between multiple risk sources and asset returns.

The factor vector $\mathbf{Y}_t \in \mathbb{R}^k$ follows a multivariate OU process:

$$d\mathbf{Y}_t = \kappa_Y (\boldsymbol{\theta}_Y - \mathbf{Y}_t) dt + \boldsymbol{\sigma}_Y d\mathbf{W}_t^Y,$$

where $\kappa_Y \in \mathbb{R}^{k \times k}$ is a mean-reversion matrix, $\boldsymbol{\theta}_Y \in \mathbb{R}^k$ is the long-run mean vector, and $\boldsymbol{\sigma}_Y \in \mathbb{R}^{k \times k}$ governs the factor volatilities and correlations (e.g., $\text{Cov}(d\mathbf{W}_t^Y) = \Phi dt$).

The n risky assets, with prices S_t^i , follow:

$$\frac{dS_t^i}{S_t^i} = \left(r + \sigma_i \boldsymbol{\alpha}_i^\top \mathbf{Y}_t \right) dt + \sigma_i dW_t^{X,i}, \quad i = 1, \dots, n.$$

Here, $\mathbf{W}_t^X \in \mathbb{R}^n$ is a Brownian motion with covariance matrix Ψdt . The asset shocks \mathbf{W}_t^X and factor shocks \mathbf{W}_t^Y can be correlated, with $\text{Cov}(dW_t^{X,i}, dW_t^{Y,j}) = \rho_{ij} dt$. Let $\rho \in \mathbb{R}^{n \times k}$ be the matrix of cross-correlations.

With portfolio weights $\boldsymbol{\pi}_t = (\pi_t^1, \dots, \pi_t^n)^\top$ and consumption C_t , wealth X_t evolves as:

$$dX_t = \left[X_t \left(r + \sum_{i=1}^n \pi_t^i \sigma_i (\boldsymbol{\alpha}_i^\top \mathbf{Y}_t) \right) - C_t \right] dt + X_t \sum_{i=1}^n \pi_t^i \sigma_i dW_t^{X,i}.$$

For CRRA utility with discount δ , the optimal consumption C_t^* depends on the wealth costate λ_t^* . The optimal portfolio $\boldsymbol{\pi}_t^* \in \mathbb{R}^n$ is given by the PMP first-order condition (Eq. (5)), which in this context becomes:

$$\boldsymbol{\pi}_t^* = - \frac{1}{X_t^* (\partial_x \lambda_t^*)} \Sigma^{-1} \left\{ \underbrace{\lambda_t^* \text{diag}(\boldsymbol{\sigma}) \mathbf{A} \mathbf{Y}_t}_{\text{Myopic Term}} + \underbrace{\text{diag}(\boldsymbol{\sigma}) \rho \boldsymbol{\sigma}_Y (\partial_{\mathbf{Y}} \lambda_t^*)^\top}_{\text{Hedging Term}} \right\},$$

where $\boldsymbol{\sigma} = (\sigma_1, \dots, \sigma_n)^\top$, $\Sigma = \text{diag}(\boldsymbol{\sigma}) \Psi \text{diag}(\boldsymbol{\sigma})$ is the $n \times n$ asset return covariance, $\mathbf{A} = (\boldsymbol{\alpha}_1, \dots, \boldsymbol{\alpha}_n)^\top$ is the $n \times k$ matrix of factor loadings, and $\partial_{\mathbf{Y}} \lambda_t^*$ is the $k \times 1$ gradient vector of the costate with respect to the factors \mathbf{Y}_t . This explicitly separates the demand into a myopic part driven by the current expected excess returns ($\text{diag}(\boldsymbol{\sigma}) \mathbf{A} \mathbf{Y}_t$) and a hedging part driven by the sensitivity to factor changes ($\partial_{\mathbf{Y}} \lambda_t^*$) and their correlations (ρ, Ψ, Φ).

Similar to the single-factor case, an analytic solution for the terminal wealth problem ($C_t = 0$) with CRRA utility can often be found using an exponential-quadratic value function ansatz, leading to matrix Riccati ODEs. Details are presented in Appendix B.2.

3 A Gradient-Based Algorithm for Multi-Asset Policy Optimization

In the preceding sections, we established the theoretical underpinnings of the continuous-time multi-asset portfolio problem using Pontryagin’s Maximum Principle (PMP). This principle provides necessary optimality conditions characterized by a coupled system of forward-backward stochastic differential equations (FBSDEs) for the state and costate variables (Section 2.2). However, finding analytical solutions to these FBSDEs is often infeasible, especially in high-dimensional settings involving numerous assets ($\boldsymbol{\pi}_t \in \mathbb{R}^n$) or complex exogenous state dynamics ($\mathbf{Y}_t \in \mathbb{R}^k$). Consequently, translating the continuous-time optimality conditions into a practical solution requires effective numerical approximations.

We adopt a *gradient-based* approach rooted in modern deep learning techniques. The core idea is to directly parameterize the investor’s policy, both the investment strategy $\boldsymbol{\pi}_t$ and the consumption rate C_t , using neural networks, denoted as $\boldsymbol{\pi}_\theta(t, x, \mathbf{y})$ and $C_\phi(t, x, \mathbf{y})$, where (θ, ϕ) are the network parameters. Optimization then involves iteratively refining these parameters to maximize the investor’s expected utility.

A key challenge is computing the gradient of the expected utility objective with respect to the policy parameters (θ, ϕ) . Furthermore, a practical policy must be effective across a relevant range of potential starting times t_0 , initial wealth levels x_0 , and initial state variable values \mathbf{y}_0 .

Let $J(t_0, x_0, \mathbf{y}_0; \theta, \phi)$ denote the conditional expected utility obtained when starting from state (t_0, x_0, \mathbf{y}_0) and following the policy defined by (θ, ϕ) :

$$J(t_0, x_0, \mathbf{y}_0; \theta, \phi) = \mathbb{E} \left[\int_{t_0}^T e^{-\delta u} U(C_\phi(u, X_u, \mathbf{Y}_u)) du + \kappa e^{-\delta T} U(X_T) \mid X_{t_0} = x_0, \mathbf{Y}_{t_0} = \mathbf{y}_0 \right]. \quad (6)$$

Here, the expectation $\mathbb{E}[\cdot]$ is taken over all possible paths of the state processes (X_u, \mathbf{Y}_u) for $u \in [t_0, T]$, conditional on starting at (x_0, \mathbf{y}_0) at time t_0 .

To ensure the policy performs well across various starting scenarios, we define the optimization target as the **extended value function**, $\tilde{J}(\theta, \phi)$. This is the expected value of the conditional utility $J(t_0, x_0, \mathbf{y}_0; \theta, \phi)$ when the initial state (t_0, x_0, \mathbf{y}_0) is drawn from a chosen distribution η over a relevant domain $\mathcal{D} \subset [0, T] \times \mathbb{R}^+ \times \mathbb{R}^k$:

$$\tilde{J}(\theta, \phi) = \mathbb{E}_{(t_0, x_0, \mathbf{y}_0) \sim \eta} \left[J(t_0, x_0, \mathbf{y}_0; \theta, \phi) \right]. \quad (7)$$

Maximizing this extended objective $\tilde{J}(\theta, \phi)$ encourages the learning of a robust policy applicable across the domain \mathcal{D} covered by the initial state distribution η .

This paper develops and implements the *Pontryagin-Guided Direct Policy Optimization (PG-DPO)* framework, extending the core ideas of Huh (2024) to the multi-asset, state-dependent setting, with the goal of maximizing the extended value function $\tilde{J}(\theta, \phi)$. The PG-DPO framework leverages automatic differentiation, specifically backpropagation-through-time (BPTT), applied to Monte Carlo simulations drawn from the initial state distribution η and evolved according to the system dynamics.

A central feature of applying BPTT in this context is that it not only provides unbiased estimates of the policy gradient $\nabla \tilde{J}$, necessary for optimizing the neural network parameters (θ, ϕ) , but also inherently calculates estimates of the Pontryagin costate variables $(\lambda_k^{(i)}, \boldsymbol{\eta}_k^{(i)})$ along each simulated path. These costates are crucial as they represent the sensitivities of the expected utility to state perturbations, as dictated by PMP.

This dual output of BPTT—policy gradients and costate estimates—allows for two distinct algorithmic approaches, both offering scalable alternatives to traditional methods hindered by the curse of dimensionality:

- The **Baseline PG-DPO** algorithm (§3.1) utilizes the BPTT-derived policy gradient estimates ($\nabla_{\text{batch}} \approx \nabla \tilde{J}$) directly within a stochastic gradient ascent procedure to train the neural network policy $(\boldsymbol{\pi}_\theta, C_\phi)$ end-to-end. In this approach, the costate estimates primarily serve to structure the gradient calculation, implicitly guiding the optimization according to PMP.

- The **Two-Stage PG-DPO** algorithm (§3.2) takes a different route. It uses the baseline procedure for a short warm-up phase specifically to generate stable and accurate estimates of the costates (potentially involving Monte Carlo averaging). These refined costate estimates are then directly plugged into the analytical first-order optimality conditions derived from PMP to define the deployed control actions, bypassing the direct use of the warm-up phase neural networks.

Both variants avoid explicit FBSDE solvers and leverage the efficiency of BPTT, but they differ significantly in how they utilize the information generated during backpropagation to arrive at the final control policy. The subsequent subsections detail each approach.

3.1 Baseline PG-DPO for the Extended Objective

The baseline PG-DPO algorithm aims to maximize the extended value function $\tilde{J}(\theta, \phi)$ (defined in Eq. (7)) using mini-batch stochastic gradient ascent. The core idea is to approximate the gradient $\nabla \tilde{J}$ by averaging gradients computed on individual sample paths, where each path starts from a randomly drawn initial state. Each iteration j of the algorithm involves the following steps:

1. **Sample Initial States:** Draw a mini-batch of M initial states $\{(t_0^{(i)}, x_0^{(i)}, \mathbf{y}_0^{(i)})\}_{i=1}^M$ from the distribution η over the domain \mathcal{D} .
2. **Simulate Forward Paths:** For each sampled initial state i , simulate a discrete-time trajectory $\{(X_k^{(i)}, \mathbf{Y}_k^{(i)})\}_{k=0}^N$ forward from $t_k = t_0^{(i)}$ to $t_N = T$, using the current policy networks $(\boldsymbol{\pi}_\theta, C_\phi)$ and correctly correlated Brownian increments $(\Delta \mathbf{W}_k^{(i),X}, \Delta \mathbf{W}_k^{(i),Y})$ derived from the Cholesky factor L of $\boldsymbol{\Sigma}_{\text{block}}$. The state evolution follows:

$$\begin{aligned} \mathbf{Y}_{k+1}^{(i)} &= \mathbf{Y}_k^{(i)} + \boldsymbol{\mu}_Y(t_k^{(i)}, \mathbf{Y}_k^{(i)})\Delta t^{(i)} + \boldsymbol{\sigma}_Y(t_k^{(i)}, \mathbf{Y}_k^{(i)})\Delta \mathbf{W}_k^{(i),Y}, \\ X_{k+1}^{(i)} &= X_k^{(i)} + \left[X_k^{(i)} \left((1 - \boldsymbol{\pi}_k^{(i)\top} \mathbf{1})r(t_k^{(i)}, \mathbf{Y}_k^{(i)}) + \boldsymbol{\pi}_k^{(i)\top} \boldsymbol{\mu}(t_k^{(i)}, \mathbf{Y}_k^{(i)}) \right) - C_k^{(i)} \right] \Delta t^{(i)} \\ &\quad + X_k^{(i)} \boldsymbol{\pi}_k^{(i)\top} \boldsymbol{\sigma}(t_k^{(i)}, \mathbf{Y}_k^{(i)})\Delta \mathbf{W}_k^{(i),X}, \end{aligned}$$

where $\Delta t^{(i)} = (T - t_0^{(i)})/N$.

3. **Calculate Realized Reward per Path:** For each path i , compute the realized cumulative reward, explicitly noting its dependence on the starting state and policy parameters, denoted as $J^{(i)}(t_0^{(i)}, x_0^{(i)}, \mathbf{y}_0^{(i)}; \theta, \phi)$:

$$J^{(i)}(t_0^{(i)}, x_0^{(i)}, \mathbf{y}_0^{(i)}; \theta, \phi) = \sum_{k=0}^{N-1} e^{-\delta t_k^{(i)}} U(C_\phi(t_k^{(i)}, X_k^{(i)}, \mathbf{Y}_k^{(i)}))\Delta t^{(i)} + \kappa e^{-\delta T} U(X_N^{(i)}).$$

This value $J^{(i)}(t_0^{(i)}, \dots)$ is a stochastic sample related to the conditional expected utility $J(t_0^{(i)}, \dots)$ defined in Eq. (6).

4. **Apply BPTT for Policy Gradient Estimate:** Treat the simulation process for path i as a computational graph. Apply automatic differentiation (BPTT) to compute the gradient of the realized reward $J^{(i)}(t_0^{(i)}, \dots)$ with respect to the policy parameters (θ, ϕ) :

$$\nabla_{(\theta, \phi)} J^{(i)}(t_0^{(i)}, x_0^{(i)}, \mathbf{y}_0^{(i)}; \theta, \phi).$$

This gradient serves as an unbiased estimate related to the gradient of the conditional expected utility $J(t_0^{(i)}, \dots)$.

5. **Estimate Gradient of \tilde{J} :** Obtain an unbiased estimate for the gradient of the overall extended objective \tilde{J} by averaging the individual path gradients over the mini-batch:

$$\nabla \tilde{J}(\theta, \phi) \approx \nabla_{\text{batch}} = \frac{1}{M} \sum_{i=1}^M \nabla_{(\theta, \phi)} J^{(i)}(t_0^{(i)}, x_0^{(i)}, \mathbf{y}_0^{(i)}; \theta, \phi).$$

6. **Update Policy Parameters:** Update the parameters (θ, ϕ) using this averaged gradient estimate via stochastic gradient ascent:

$$(\theta, \phi)_{j+1} \leftarrow (\theta, \phi)_j + \alpha_j \nabla_{\text{batch}},$$

where α_j is the learning rate.

By iterating these steps, the baseline PG-DPO algorithm gradually optimizes the policy (π_θ, C_ϕ) to maximize the extended value function J .

Role of Intermediate BPTT Values and the ‘‘Pontryagin-Guided’’ Nature. It is important to understand the role of the intermediate values computed during BPTT in Step 4. As BPTT calculates the policy gradient $\nabla J^{(i)}(\dots)$ via the chain rule, it inherently computes the partial derivatives of the realized reward $J^{(i)}(\dots)$ with respect to the intermediate states along path i :

$$\lambda_k^{(i)} = \frac{\partial J^{(i)}(t_0^{(i)}, \dots)}{\partial X_k^{(i)}}, \quad \boldsymbol{\eta}_k^{(i)} = \frac{\partial J^{(i)}(t_0^{(i)}, \dots)}{\partial \mathbf{Y}_k^{(i)}}.$$

These values, $\lambda_k^{(i)}$ and $\boldsymbol{\eta}_k^{(i)}$, are unbiased estimates of the Pontryagin costates associated with the conditional expected utility $J(t_0^{(i)}, \dots)$. Crucially, in the *baseline*

PG-DPO algorithm, these costate estimates themselves (and their potential derivatives w.r.t. states) are **not directly used** in the parameter update rule (Step 6), which only requires the final gradient $\nabla_{(\theta,\phi)} J^{(i)}(\dots)$.

Nevertheless, the fact that BPTT provides access to these estimates is fundamental. Firstly, they are essential inputs for the **Two-Stage PG-DPO** variant discussed in the next subsection (§3.2). The baseline algorithm thus lays the groundwork by generating these estimates. Secondly, this connection explains why the algorithm is termed **Pontryagin-Guided**. Even though the baseline update only uses $\nabla J^{(i)}(\dots)$, the calculation of this gradient via BPTT structurally mirrors the backward propagation of sensitivities inherent in PMP’s adjoint equations, using the costate estimates $\lambda_k^{(i)}, \boldsymbol{\eta}_k^{(i)}$ implicitly within the chain rule (cf. Huh, 2024). Therefore, the optimization process, driven by these BPTT-computed gradients, is implicitly guided by the optimality conditions derived from Pontryagin’s principle, aiming to maximize the expected objective \tilde{J} .

3.2 Two-Stage PG-DPO Algorithm

While the baseline PG-DPO algorithm described in Section 3.1 effectively optimizes the extended objective \tilde{J} by training the policy networks $(\boldsymbol{\pi}_\theta, C_\phi)$ end-to-end, it can sometimes require a significant number of iterations for the networks to fully converge. The Two-Stage PG-DPO variant offers a potentially more computationally efficient alternative by exploiting an empirical observation: the costate estimates $(\lambda_k^{(i)}, \boldsymbol{\eta}_k^{(i)})$ and their relevant derivatives with respect to states, like $\partial_x \lambda_k^{(i)}, \partial_{\mathbf{Y}} \lambda_k^{(i)}$, which are generated during BPTT, often stabilize and become reasonably accurate much faster than the full policy networks achieve optimality.

This Two-Stage approach leverages these rapidly stabilizing costate estimates to construct near-optimal controls directly from the PMP first-order conditions, bypassing the need for fully converged policy networks for deployment. The procedure consists of two distinct stages, described below using a single level of enumeration:

1. Stage 1: Warm-Up Phase for Costate Estimation

First, we execute the **Baseline PG-DPO process**, as detailed in Section 3.1 (which optimizes \tilde{J}), for a predetermined, relatively small number of iterations, K_0 . The primary objective of this stage is **not** to obtain fully optimized networks $(\boldsymbol{\pi}_\theta, C_\phi)$, but rather to run the BPTT process sufficiently long for the underlying mechanism generating the **costate estimates** $(\lambda_k^{(i)} = \partial J^{(i)}(\dots)/\partial X_k^{(i)}, \boldsymbol{\eta}_k^{(i)} = \partial J^{(i)}(\dots)/\partial \mathbf{Y}_k^{(i)})$ and their relevant state-derivatives (e.g., $\partial_x \lambda_k^{(i)}, \partial_{\mathbf{Y}} \lambda_k^{(i)}$) to stabilize. We let (θ^*, ϕ^*) denote the policy parameters obtained at the end of this warm-up phase.

2. Stage 2: Analytic Control Deployment

After completing the K_0 warm-up iterations, the trained policy networks $(\boldsymbol{\pi}_{\theta^*}, C_{\phi^*})$ are typically **not directly used** for generating controls during deployment. Instead, to determine the control actions for any given state (t_k, X_k, \mathbf{Y}_k) encountered during deployment, we employ a Monte Carlo-like averaging procedure to obtain reliable costate estimates needed for the PMP formulas:

First, to obtain the **stabilized costate estimates** corresponding to the state (t_k, X_k, \mathbf{Y}_k) , we perform the following averaging: Simulate multiple (M_{MC}) forward paths starting from (t_k, X_k, \mathbf{Y}_k) (or states very close to it) up to the horizon T , using the *fixed* policy parameters (θ^*, ϕ^*) obtained from Stage 1. For each simulated path $j = 1, \dots, M_{\text{MC}}$, calculate its realized reward $J^{(j)}(t_k, X_k, \mathbf{Y}_k; \theta^*, \phi^*)$ and apply BPTT to obtain the costate estimates $\lambda_k^{(j)}, \partial_x \lambda_k^{(j)}, \partial_{\mathbf{Y}} \lambda_k^{(j)}$ specifically at the starting node k for that path j . The final “stabilized” estimates are then computed by averaging these values across the M_{MC} paths:

$$\lambda_k \approx \frac{1}{M_{\text{MC}}} \sum_{j=1}^{M_{\text{MC}}} \lambda_k^{(j)}, \quad \partial_x \lambda_k \approx \frac{1}{M_{\text{MC}}} \sum_{j=1}^{M_{\text{MC}}} \partial_x \lambda_k^{(j)}, \quad \partial_{\mathbf{Y}} \lambda_k \approx \frac{1}{M_{\text{MC}}} \sum_{j=1}^{M_{\text{MC}}} \partial_{\mathbf{Y}} \lambda_k^{(j)}$$

This averaging acts as a Monte Carlo estimation step, significantly reducing the variance inherent in the single-path BPTT estimates derived during Stage 1 and providing more robust inputs for the PMP formulas.

Next, we plug these **averaged costate estimates** $(\lambda_k, \partial_x \lambda_k, \partial_{\mathbf{Y}} \lambda_k)$ directly into the analytical formulas derived from the Pontryagin Maximum Principle’s first-order conditions (Section 2.2). The optimal consumption is calculated as:

$$C_k^{\text{PMP}} = (U')^{-1}(e^{\delta t_k} \lambda_k).$$

The optimal investment portfolio is calculated as:

$$\boldsymbol{\pi}_k^{\text{PMP}} = - \frac{1}{X_k (\partial_x \lambda_k)} \Sigma(t_k, \mathbf{Y}_k)^{-1} \left\{ \underbrace{\lambda_k [\boldsymbol{\mu}(t_k, \mathbf{Y}_k) - r(t_k, \mathbf{Y}_k) \mathbf{1}]}_{\text{Myopic Demand}} + \underbrace{\boldsymbol{\sigma}(t_k, \mathbf{Y}_k)^\top [(\partial_{\mathbf{Y}} \lambda_k) \boldsymbol{\sigma}_Y(t_k, \mathbf{Y}_k) \rho^\top \Psi^{-1}]}_{\text{Hedging Demand}} \right\}.$$

Finally, these analytically computed values $(C_k^{\text{PMP}}, \boldsymbol{\pi}_k^{\text{PMP}})$, based on the averaged costate estimates, are used as the control actions for the state (t_k, X_k, \mathbf{Y}_k) during deployment.

In summary, the Two-Stage PG-DPO approach performs a short warm-up training (Stage 1) using the baseline PG-DPO process to obtain a policy (θ^*, ϕ^*) whose BPTT generates reasonably stable costate estimates. It then leverages these estimates in Stage 2, refining them through Monte Carlo averaging at the point of deployment and plugging them into the known analytical structure of the optimal control derived from PMP. This strategy can significantly reduce the overall computational burden while yielding high-quality, near-optimal controls. The Monte Carlo averaging step in Stage 2 is crucial for obtaining reliable inputs for the PMP formulas from the potentially noisy single-path estimates.

3.3 Rationale for the Two-Stage Approach: Leveraging Costate Estimation

The preceding subsections introduced two variants of the PG-DPO framework: a baseline approach (§3.1) and a Two-Stage approach (§3.2). A natural question arises: why introduce the Two-Stage variant, which potentially adds complexity, instead of solely relying on optimizing the policy networks directly? This subsection elaborates on the theoretical and practical motivations.

3.3.1 Qualitative Rationale: Exploiting PMP Structure and Costate Properties

At its core, the rationale stems from the structure provided by Pontryagin’s Maximum Principle (PMP) itself and the economic meaning of the costate variables. As established in Section 2.2, PMP characterizes the optimal controls (π_t^*, C_t^*) directly in terms of the costates (λ_t^*, η_t^*) and their relevant derivatives (e.g., $\partial_x \lambda_t^*$, $\partial_{\mathbf{Y}} \lambda_t^*$). The analytical formulas used in Stage 2 of the Two-Stage method are precisely these first-order conditions. Therefore, if accurate estimates of these costates and their derivatives could be obtained, PMP provides a direct blueprint for constructing the optimal policy.

Furthermore, the primary costate λ_t represents the marginal utility of wealth ($\lambda_t \approx \partial V / \partial x$). Economic principles, like consumption smoothing, suggest agents strive for a stable marginal utility path. Mathematically, this often means the value function V and its derivatives (λ_t , $\partial_x \lambda_t$, $\partial_{\mathbf{Y}} \lambda_t$, etc.) exhibit relatively smooth behavior or possess a simpler analytical structure compared to the optimal policy functions (π^*, C^*) themselves. The optimal policy might need to be highly complex, especially in non-affine settings or under constraints.

This difference in potential complexity has direct implications for learning dynamics. It is plausible that learning the potentially smoother or more structured functions associated with the costates via BPTT during the warm-up phase (Stage 1) is an easier task-requiring fewer iterations for stabilization-than learning the full

complexity of the optimal policy networks $(\boldsymbol{\pi}_\theta, C_\phi)$ until convergence. This aligns with empirical observations that costate estimates often stabilize relatively quickly.

The potential for faster convergence or stabilization of costate-related functions compared to the full policy motivates the Two-Stage approach. This is further encouraged, albeit heuristically for general models, by theoretical stability results known for specific structured models, as formalized in the next subsection.

3.3.2 Derivative Stability in Structured Models

For certain classes of portfolio choice problems that admit explicit solutions, such as those within affine or quadratic frameworks, a strong link exists between the accuracy of the value function approximation and the accuracy of its derivatives, provided the approximation retains the original structure. This property is formally stated as follows:

Proposition 3.1 (Derivative Closeness from Value Closeness in Structured Models). *Consider a class of portfolio choice models (e.g., Merton with HARA utility (Merton, 1971), Kim & Omberg with HARA utility (Kim & Omberg, 1996), or Liu’s affine/quadratic framework with CRRA utility (Liu, 2007)) where the optimal value function $V^*(t, w, \mathbf{y})$ has a known analytical structure (e.g., separable or exponential-polynomial in state variables with coefficients determined by ODEs). Let $\tilde{V}(t, w, \mathbf{y})$ be another function defined on a compact domain $\mathcal{D} \subset [0, T] \times \mathbb{R}^+ \times \mathbb{R}^k$ that shares the **same analytical structure** as V^* . If the value functions are uniformly close on \mathcal{D} , i.e.,*

$$\sup_{(t, w, \mathbf{y}) \in \mathcal{D}} |V^*(t, w, \mathbf{y}) - \tilde{V}(t, w, \mathbf{y})| \rightarrow 0,$$

then their corresponding spatial derivatives (first and second order with respect to w and \mathbf{y}) also converge uniformly on \mathcal{D} :

$$\sup_{\mathcal{D}} \|\nabla_{w, \mathbf{y}} V^* - \nabla_{w, \mathbf{y}} \tilde{V}\| \rightarrow 0 \quad \text{and} \quad \sup_{\mathcal{D}} \|\nabla_{w, \mathbf{y}}^2 V^* - \nabla_{w, \mathbf{y}}^2 \tilde{V}\| \rightarrow 0.$$

(Proof sketch provided in Appendix C for the Liu (2007) framework).

Implication for PG-DPO Rationale. Proposition 3.1 highlights that for well-structured problems (like those within the affine class for which the proposition holds), the derivatives inherent in the PMP conditions are well-behaved with respect to approximations that preserve the specific analytical structure. However, a key motivation for employing methods like PG-DPO is their potential applicability to a **broader class of problems, including models that may lack such convenient structures** — for instance, models involving **non-affine dynamics**

(such as the CEV examples considered later in this paper). The true optimal value function V^* for these more general models may not possess the specific separable or exponential-polynomial form assumed in the proposition.

Consequently, Proposition 3.1, proven for specific structured models, does not directly guarantee that similar derivative stability holds for the **wider range of potentially non-affine models** that PG-DPO aims to tackle. Establishing whether analogous stability properties exist in these more general settings, or rigorously proving the convergence of derivative estimates obtained via BPTT from neural network approximations in such cases, remains an area for future research and is beyond the scope of this paper.

Nevertheless, the proposition provides valuable context. It confirms that the target objects (optimal value function derivatives) possess inherent stability within important, albeit specific, classes of models. This offers **heuristic support** for the hypothesis underlying the Two-Stage PG-DPO: namely, that the costate derivatives, being fundamental quantities in a well-posed optimal control problem, might be estimated reliably via BPTT (Stage 1) and effectively used in the PMP formulas (Stage 2), **even when tackling more complex, potentially non-affine models**.

4 Numerical Experiments

In this section, we conduct numerical experiments to evaluate the performance and scalability of the proposed PG-DPO framework (both Baseline and Two-Stage variants). To enable rigorous comparison with the available semi-analytical benchmark for the terminal wealth problem (Appendix B.2), the numerical experiments presented herein focus exclusively on maximizing $J = \mathbb{E}[U(X_T)]$. Consequently, the optimization of the intermediate consumption policy C_ϕ , though supported by the general framework (Sections 2-3), is omitted in this study. We focus on the multi-asset, multi-factor portfolio optimization problem introduced in Section 2.3.2. As detailed therein, this specific model involves n risky assets whose expected returns are driven by k correlated Ornstein-Uhlenbeck (OU) state variables \mathbf{Y}_t .

Crucially, this model specification falls within the affine class. This allows us to compute a semi-analytical benchmark solution by solving a system of Riccati-type ordinary differential equations (ODEs), as outlined in Appendix B.2. This benchmark provides a basis for rigorously comparing the accuracy of the PG-DPO methods.

4.1 Experimental Setup

4.1.1 Parameter Values

The experiments consider the objective of maximizing the expected utility of terminal wealth X_T , $J = \mathbb{E}[U(X_T)]$, using a CRRA utility function $U(x) = x^{1-\gamma}/(1-\gamma)$ with a relative risk aversion coefficient $\gamma = 2.0$. The fixed time horizon is $T = 1.5$.

Unless otherwise specified, the model parameters (for the model described in Section 2.3.2) are generated based on the asset dimension n and factor dimension k using the following process (seeded for reproducibility, e.g., ‘seed=42’):

- Risk-free rate: $r = 0.03$.
- State process parameters (for the k -dimensional OU process \mathbf{Y}_t):
 - Mean-reversion speeds: $\boldsymbol{\kappa}_Y = \text{diag}(2.0, 2.5, \dots, 2.0 + (k - 1)0.5)$.
 - Long-term means: $\boldsymbol{\theta}_Y$ components drawn uniformly from $U(0.2, 0.4)$.
 - Factor volatilities: $\boldsymbol{\sigma}_Y$ diagonal elements drawn uniformly from $U(0.3, 0.5)$.
- Asset parameters (for the n risky assets):
 - Volatilities: $\boldsymbol{\sigma} \in \mathbb{R}^n$ components drawn uniformly from $U(0.1, 0.5)$.
 - Factor loadings: $\boldsymbol{\alpha} \in \mathbb{R}^{n \times k}$ drawn using ‘scipy.stats.dirichlet’ with concentration parameters $[1.0, \dots, 1.0]$. (Note: These define the risk premium structure $\boldsymbol{\mu} = r\mathbf{1} + \text{diag}(\boldsymbol{\sigma})\boldsymbol{\alpha}\mathbf{Y}_t$).
- Correlation structure: The generation process aims to produce realistic correlation parameters while ensuring the overall block correlation matrix remains positive definite, which is crucial for stable simulations. This involves:
 - Asset correlation Ψ ($n \times n$) generated based on a latent factor structure ensuring validity.
 - Factor correlation Φ_Y ($k \times k$) generated as a random correlation matrix.
 - Cross-correlation $\boldsymbol{\rho}_Y$ ($n \times k$) components drawn uniformly from $U(-0.2, 0.2)$.
 - The full $(n + k) \times (n + k)$ block correlation matrix $\begin{pmatrix} \Psi & \boldsymbol{\rho}_Y \\ \boldsymbol{\rho}_Y^\top & \Phi_Y \end{pmatrix}$ is constructed and numerically adjusted (e.g., via minimal diagonal loading) if necessary to ensure positive definiteness (tolerance 10^{-6}).

The specific values generated by the seed are used consistently across experiments for given n and k .

4.1.2 PG-DPO Implementation Details

We implement the Baseline PG-DPO algorithm using PyTorch.

- **Policy Network (π_θ):** The policy network architecture consists of an input layer taking the current wealth W_t , current time t , and state vector \mathbf{Y}_t (total $2 + k$ inputs), followed by three hidden layers with 200 units each and LeakyReLU activation, and an output layer producing the n -dimensional portfolio weight vector π_θ .
- **Optimizer:** Adam optimizer with a learning rate of 1×10^{-5} .
- **Training:**

- Total epochs: 10,000.
- Batch size (M): 1,000.
- Time discretization steps (N): 20.
- Initial state sampling (η): For each trajectory in a batch, the initial time t_0 is drawn uniformly from $[0, T)$, initial wealth W_0 from $U(0.1, 3.0)$. The initial state variables $\mathbf{Y}_0 = (Y_{0,1}, \dots, Y_{0,k})^\top$ are sampled such that each component $Y_{0,i}$ is drawn independently and uniformly from a single common range $[Y_{\min}, Y_{\max}]$. This range is determined by the minimum lower bound and the maximum upper bound observed across all individual factors’ typical $\pm 3\sigma$ intervals:

$$Y_{\min} = \min_{i=1, \dots, k} (\theta_{Y,i} - 3\sigma_{Y,ii}), \quad Y_{\max} = \max_{i=1, \dots, k} (\theta_{Y,i} + 3\sigma_{Y,ii}),$$

where $\theta_{Y,i}$ is the long-term mean and $\sigma_{Y,ii}$ is the instantaneous volatility parameter for the i -th factor. The simulation then runs forward from t_0 to the fixed horizon T using $N = 20$ time steps, with step size $\Delta t = (T - t_0)/N$. This approach ensures the policy is trained effectively across the entire time interval $[0, T]$ and a relevant hypercube in the state space defined by the collective factor dynamics.

- Variance Reduction: Antithetic variates used.
- Wealth constraint: Simulated wealth W_t clamped at lower bound 0.1.
- **Costate Estimation (for Two-Stage Evaluation):** During periodic evaluation, costate λ and derivatives $\partial_x \lambda, \partial_{\mathbf{Y}} \lambda$ are computed via BPTT (‘torch.autograd.grad’) applied to Monte Carlo estimates of the expected terminal utility starting from evaluation points (t_k, W_k, \mathbf{Y}_k) .

4.1.3 Benchmark Solution and Evaluation

As mentioned, the chosen multi-factor OU model allows for a semi-analytical benchmark solution. It is important to note that these experiments focus solely on the terminal wealth objective ($J = \mathbb{E}[U(X_T)]$), and thus do not include optimization or a neural network for the consumption policy C_ϕ . This simplification is made specifically to enable direct comparison with the semi-analytical benchmark solution derived from the HJB equation, which is readily available for the terminal wealth problem in this affine setting.

- **Benchmark Computation:** The system of ODEs (including a matrix Riccati equation) associated with the HJB equation for this terminal wealth problem (Appendix B.2) is solved numerically backwards from the fixed horizon T using ‘scipy.integrate.solve_ivp’ (‘Radau’ method) to obtain the coefficients determining the value function and the optimal policy $\pi^*(t, W_t, \mathbf{Y}_t)$.
- **Interpolation:** The benchmark policy (total, myopic, and hedging components) is pre-computed on a grid over (t, W_t, \mathbf{Y}_t) space and stored using ‘scipy.interpolate.RegularGridInterpolator’ for efficient lookup.
- **Evaluation Metrics:** Performance is evaluated via the Root Mean Squared Error (RMSE) between the policies generated by (i) Baseline PG-DPO (π_θ) and the benchmark (π^*), and (ii) Two-Stage PG-DPO (using Eq. (5) with BPTT-estimated costates) and the benchmark (π^*). RMSEs are computed for total, myopic, and hedging components.
- **Visualization:** Contour plots compare the learned policies and the benchmark over the state space (typically time t vs. one state variable Y_k), alongside error plots and costate visualizations.

All computations are performed using PyTorch on an NVIDIA A6000 GPU.

4.2 Convergence Speed and Accuracy Analysis

This section quantitatively compares the convergence speed and final accuracy of the proposed PG-DPO methodologies across various dimensional settings. Figure 1 displays the Root Mean Squared Error (RMSE) between the learned policies (either π_θ for Baseline PG-DPO or π^{PMP} for Two-Stage PG-DPO) and the benchmark optimal policy (π^*) as a function of training epochs, plotted on a logarithmic scale. The results are shown for configurations of (a) $n=1$ asset, $k=10$ state variables, (b) $n=10$, $k=10$, and (c) $n=50$, $k=10$.

The RMSE for the Two-Stage PG-DPO (orange line in Figure 1) represents the error of the total portfolio policy π^{PMP} constructed by substituting the costate

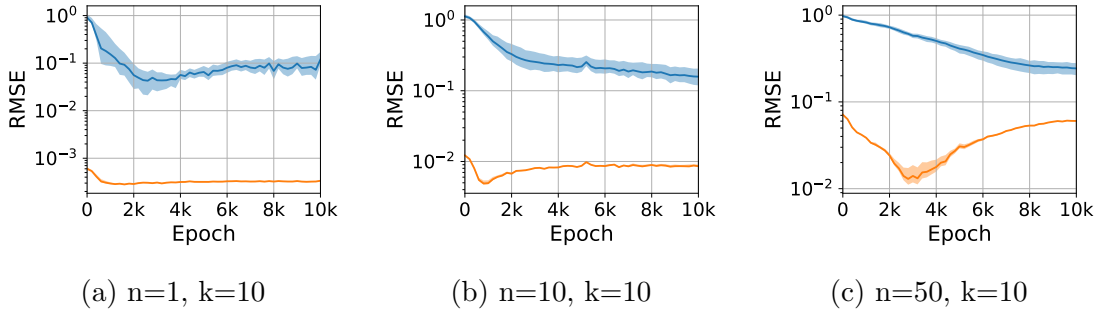


Figure 1: RMSE comparison between Baseline PG-DPO (blue) and Two-Stage PG-DPO (orange) policies relative to the benchmark solution across different dimensions. Note the logarithmic scale on the y-axis.

estimates obtained via BPTT at each epoch into the PMP first-order condition (Eq. (5)). A key advantage, and distinction from the Baseline PG-DPO which learns the total policy π_θ monolithically, is that the Two-Stage approach explicitly computes the policy by combining the analytically distinct *myopic* and *hedging* components derived from the PMP formula. This allows for separate assessment of their accuracy. As established theoretically for affine models with CRRA utility (Appendix B) and confirmed in preliminary component-wise error analyses, the error associated with the myopic component (driven by the ratio $-\lambda_t^*/(X_t^* \partial_x \lambda_t^*) = 1/\gamma$) is typically negligible and converges almost instantly. Therefore, the total RMSE observed for the Two-Stage PG-DPO policy (orange line in Figure 1) is **almost entirely attributable to the error in estimating the hedging component**. The remarkably low overall error achieved by the Two-Stage method thus highlights its proficiency in accurately capturing this crucial, often complex, hedging demand using BPTT-derived costate derivatives ($\partial_{\mathbf{Y}} \lambda_t^*$).

The key finding, consistently observed across all cases presented in Figure 1, is that the **Two-Stage PG-DPO (orange) converges significantly faster and achieves a substantially lower final (or minimum) RMSE compared to the Baseline PG-DPO (blue)**. This clearly demonstrates the superiority of the Two-Stage approach, which leverages costate estimates derived from BPTT to reconstruct the policy according to the PMP structure.

Analyzing each case provides further insights:

- **$n=1, k=10$ (Figure 1a):** In this scenario with numerous state variables, the Two-Stage method converges rapidly within approximately 1,000 epochs to a very low RMSE level of around 3×10^{-3} . In contrast, the Baseline method converges much slower, stabilizing after about 4,000 epochs at a significantly higher RMSE level of approximately 7×10^{-2} . This results in a

substantial gap (over 20-fold) in the final accuracy between the two methods.

- **n=10, k=10 (Figure 1b):** A similar trend persists in this intermediate-scale case with an increased number of assets. The Two-Stage method still converges quickly, reaching an RMSE of about 1.5×10^{-2} within roughly 2,000 epochs, whereas the Baseline method exhibits slower convergence and achieves a less accurate result with an RMSE around 1×10^{-1} .
- **n=50, k=10 (Figure 1c):** For this most complex, high-dimensional case, training was conducted only up to 3,000 epochs. Nevertheless, the performance difference is stark. The Two-Stage method displays much faster initial convergence, reaching a minimum RMSE of approximately 1.5×10^{-2} near the 3,000-epoch mark. Although a slight tendency for the error to increase afterward is observed—potentially indicating the need for a longer warm-up phase (Stage 1) or suggesting instability in costate estimates requiring further training or tuning—its achieved accuracy is remarkable. Considering that the Baseline method’s RMSE is still above 2×10^{-1} at the same 3,000-epoch point, we can conclude that **the Two-Stage approach yields a significantly more accurate policy within the same computational budget.**

These results strongly support the rationale behind the Two-Stage approach discussed in Section 3.3. Specifically, BPTT can effectively estimate the necessary costate information (particularly its derivatives) required by the PMP conditions with relatively few training iterations. Integrating these estimates into the analytical structure provided by the PMP optimality conditions proves to be more efficient and accurate than attempting to directly approximate the complex optimal policy function end-to-end using a neural network (Baseline approach), especially as the problem dimensionality increases.

Building upon this quantitative analysis, the subsequent sections will provide visual comparisons of the policy functions for specific cases via contour plots, offering further insights into the qualitative differences between the policies generated by the two methods. Hereafter, we often abbreviate Two-Stage PG-DPO as 2-PG-DPO for brevity

4.3 Detailed Analysis for the Single-Asset, Single-Factor Case (n=1, k=1)

We begin with a detailed examination of the simplest state-dependent setting (n=1, k=1) to visually validate the methodologies and illustrate the structure of the learned policies. The results presented in this subsection correspond to the state of the policies after 2,000 training epochs, a point observed to be near optimal

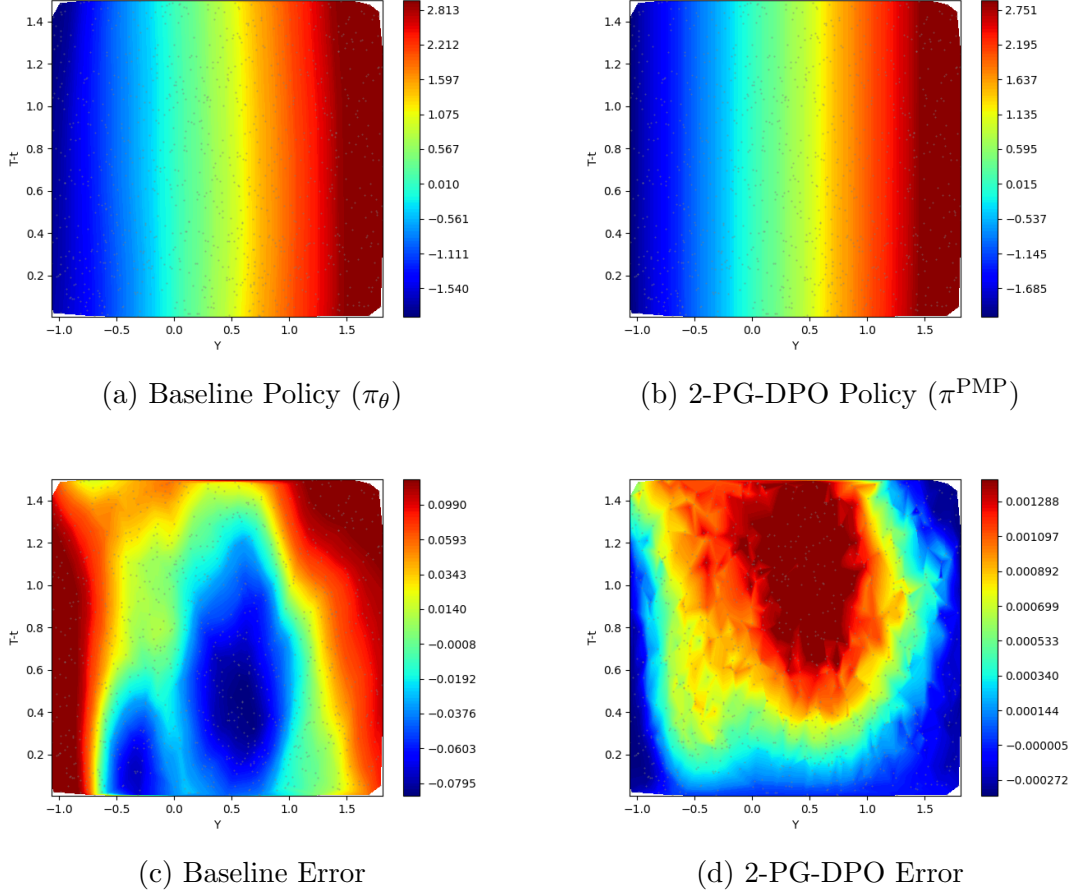


Figure 2: Comparison of total policies and errors for the $n=1, k=1$ case at epoch 2000. Top row compares the policies from Baseline PG-DPO (left) and 2-PG-DPO (right). Bottom row compares their respective errors. Note the significantly different color bar scales for the error plots.

for the 2-PG-DPO method in this configuration (cf. Figure 1a) before potential performance degradation with extended training, as discussed later.

Figure 2 compares the total policies learned by the Baseline PG-DPO and 2-PG-DPO methods, alongside their respective errors relative to the benchmark solution. Figure 3 then decomposes the superior 2-PG-DPO policy into its constituent myopic and hedging components, showing their individual shapes and associated errors. All plots show the policy or error values against time-to-maturity ($T - t$) and the state variable (Y).

Observing Figure 2, we compare the Baseline PG-DPO policy (2a) and its error (2c) with the 2-PG-DPO policy (2b) and its error (2d). While the Baseline

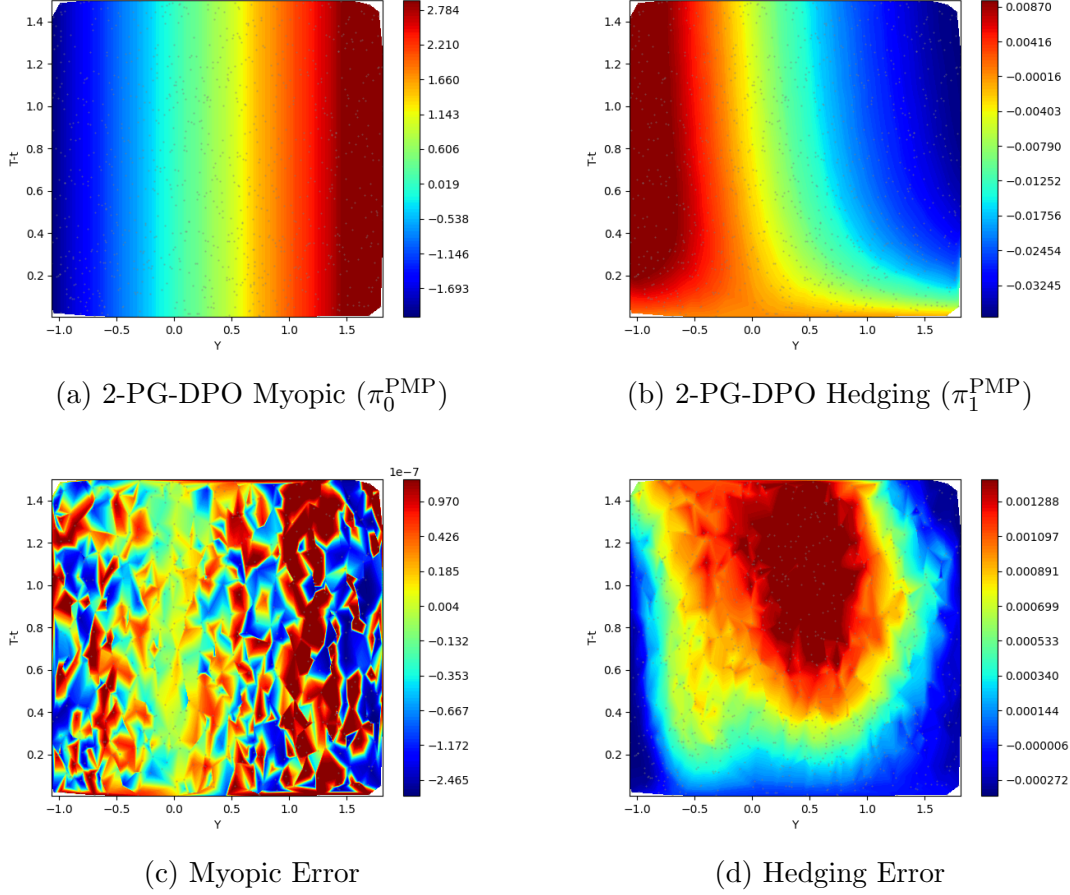


Figure 3: Decomposition of the 2-PG-DPO policy for the $n=1, k=1$ case at epoch 2000. Top row shows the myopic (left) and hedging (right) components. Bottom row shows their respective errors. Note the extremely small error scale for the myopic component.

network learns the general dependency on the state variable Y , its error plot (2c) reveals significant deviations from the benchmark, with magnitudes reaching up to $\approx \pm 0.1$. This visual representation aligns with the relatively high RMSE seen for the Baseline method around epoch 2000 in Figure 1a. Although this error level is considerably higher than that of the 2-PG-DPO method even in this simple $n=1, k=1$ setting, it represents the performance in the simplest possible setting. It is crucial to emphasize that the effectiveness of the Baseline PG-DPO approach tends to diminish considerably as the number of assets (n) and state variables (k) grows. The challenge of directly approximating the increasingly complex optimal policy function often becomes intractable for the Baseline method in higher dimensions,

leading to much larger errors or convergence difficulties, as hinted by the widening gap in RMSE observed in Figure 1 for larger n . Therefore, while the Baseline method shows some learning capability here, its limitations in scalability motivate the need for more robust approaches like 2-PG-DPO for the high-dimensional problems central to this paper. In stark contrast, the 2-PG-DPO policy (2b) yields a drastically reduced error (2d), with magnitudes mostly within $\approx \pm 0.001$, corresponding well with its low RMSE and suggesting close proximity to the true optimal solution, demonstrating its effectiveness even in this simple case.

Figure 3 provides crucial insights into the superior performance of the 2-PG-DPO method by decomposing its policy. The myopic component (3a) is visually dominant. Crucially, its associated error (3c) is extremely small (order 10^{-7}), confirming its near-perfect accuracy. The hedging component (3b), representing a smaller adjustment, has an associated error (3d) that is visually identical in pattern and magnitude (order 10^{-3}) to the total error of the 2-PG-DPO policy (2d). This visually confirms that the overall accuracy of the 2-PG-DPO policy is primarily limited by the accuracy of estimating the hedging demand.

Finally, it is important to address the training duration and the potential for overfitting with the 2-PG-DPO method. While this method achieves high accuracy remarkably quickly (around 2000 epochs here, corresponding to only about 5-10 minutes of computation time, given that 10,000 epochs take approximately 30 minutes on the utilized NVIDIA A6000 GPU), we observed that continued training beyond this near-optimal point can lead to a degradation of its performance (i.e., an increase in RMSE, as hinted in Figure 1a). This phenomenon might suggest that the underlying neural network used for costate estimation during the warm-up phase (Stage 1) could potentially start to overfit to the specific discrete time steps ($\Delta t > 0$) and sample paths inherent in the simulation-based training [cite: 293]. Instead of learning the true continuous-time (dt) value function derivatives needed for the PMP formulas, the network might adapt too closely to the artifacts of the discretization. This underscores the importance of careful monitoring and potentially early stopping for the warm-up phase—which requires only a short computational time—to extract the best performance from the 2-PG-DPO methodology.

In summary, the analysis for the $n=1, k=1$ case visually confirms the high accuracy of the 2-PG-DPO approach compared to the Baseline PG-DPO, clearly illustrates the decomposition into highly accurate myopic and less accurate (but still relatively small error) hedging components, and underscores the significance of selecting an appropriate training duration for optimal performance.

4.4 Analysis with Multiple State Variables (n=1, k=10)

We now increase the complexity by considering a case with a single asset but numerous state variables (n=1, k=10). This scenario tests the ability of the methods to handle high-dimensional state dependencies that affect the investment opportunity set. As visualizing the full 10-dimensional state dependency is impossible, the following plots (Figures 4 and 5) display the policy and error values as functions of time-to-maturity ($T - t$) and the first state variable (Y_1), while holding the remaining state variables (Y_2, \dots, Y_{10}) constant at their respective long-term mean values ($\theta_{Y,i}$). The results shown correspond to 2,000 training epochs, consistent with the previous analysis. The overall convergence for this case is depicted in Figure 1a.

Figure 4 presents the comparison for the n=1, k=10 case. The Baseline PG-DPO policy (4a) again learns the dependency on the displayed state variable Y_1 . However, its error relative to the benchmark (4c) remains significant, with magnitudes ranging roughly between 0.001 and 0.064. This level of error is consistent with the high RMSE value observed for the Baseline method in Figure 1a, indicating difficulties in accurately capturing the complex policy function influenced by ten state variables. This difficulty highlights a key challenge for the Baseline PG-DPO approach, particularly when the number of state variables (k) is large. The network must learn to approximate the total policy, which implicitly combines the primary myopic demand with the complex intertemporal hedging demands arising from all ten state variables (Y_1, \dots, Y_{10}). Even if the magnitude of the hedging component related to any single factor or the total hedging demand itself is relatively small (as suggested by Figure 5b for the Y_1 dimension), the sheer number of interacting hedging influences creates a highly intricate functional relationship for the optimal policy. Attempting to capture this subtle, high-dimensional structure directly through gradient updates on a single policy network can disrupt the learning process. This may hinder convergence towards the true optimum or even lead to the network converging to an inaccurate or distorted policy shape, as potentially reflected in the structured errors seen in Figure 4c. Conversely, the 2-PG-DPO method, by explicitly utilizing the PMP structure and separating the estimation of terms related to λ and its derivatives ($\partial_{\mathbf{Y}}\lambda$), demonstrates remarkable accuracy even in this high-dimensional state setting. The total policy (4b) results in an extremely small error (4d), with magnitudes only reaching up to approximately 3.6×10^{-4} . This visually confirms the near-perfect fit suggested by the very low RMSE value achieved by the 2-PG-DPO method shown in Figure 1a, showcasing its ability to effectively handle a large number of state factors.

Figure 5 provides further validation through the decomposition of the 2-PG-DPO policy. The myopic component (5a) largely determines the shape of the total policy. Its corresponding error (5c) remains negligible, on the order of 10^{-7} , prov-

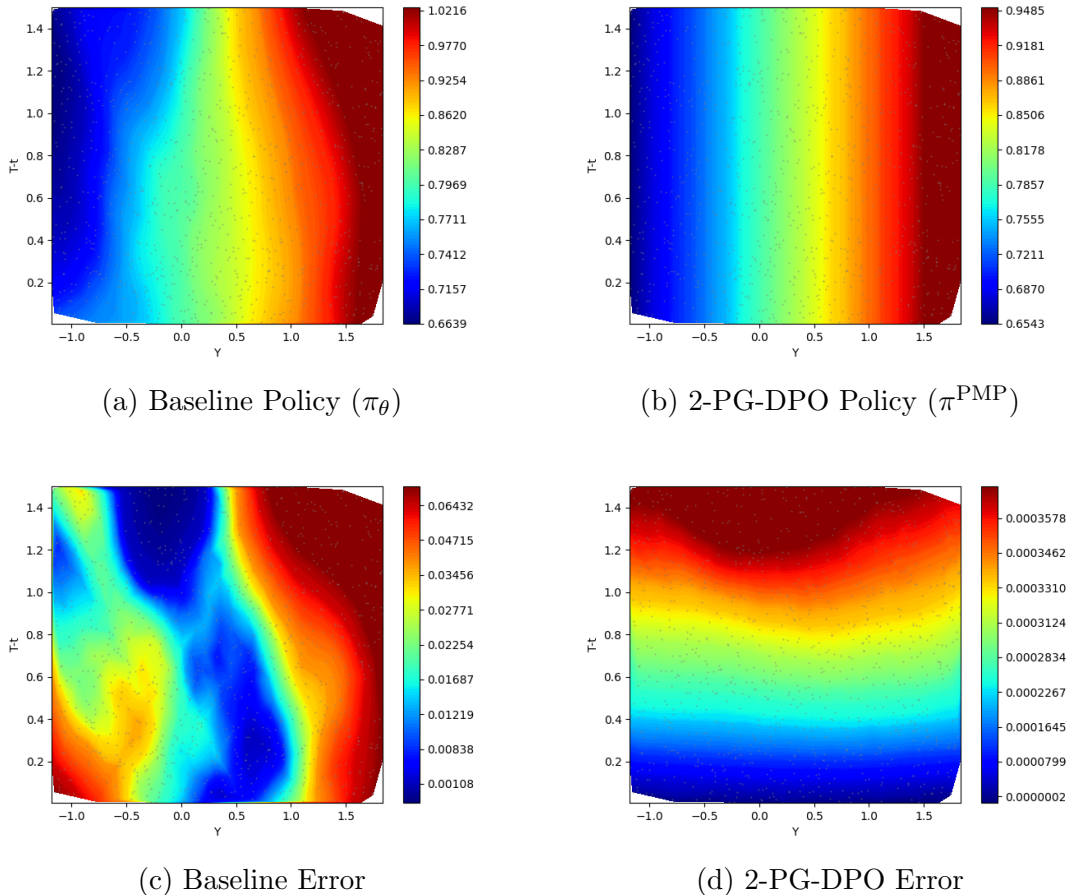


Figure 4: Comparison of total policies and errors for the $n=1, k=10$ case at epoch 2000 (plotted against Y_1). Top row compares the policies from Baseline PG-DPO (left) and 2-PG-DPO (right). Bottom row compares their respective errors. Note the significantly different color bar scales for the error plots.

ing its accurate estimation. The hedging component (5b) is exceptionally small in this particular slice (magnitude order 10^{-4}), suggesting that for this specific configuration and visualization plane, the intertemporal hedging demand related to Y_1 is minimal. Nevertheless, the error associated with this tiny hedging component (5d) is again visually identical to the total error of the 2-PG-DPO policy (4d), confirming that the overall policy accuracy is still dictated by the precision of the hedging term estimation, even when this term (and its error) is extremely small.

In conclusion, the results for the $n=1, k=10$ case demonstrate the robustness and high accuracy of the 2-PG-DPO method when faced with high-dimensional

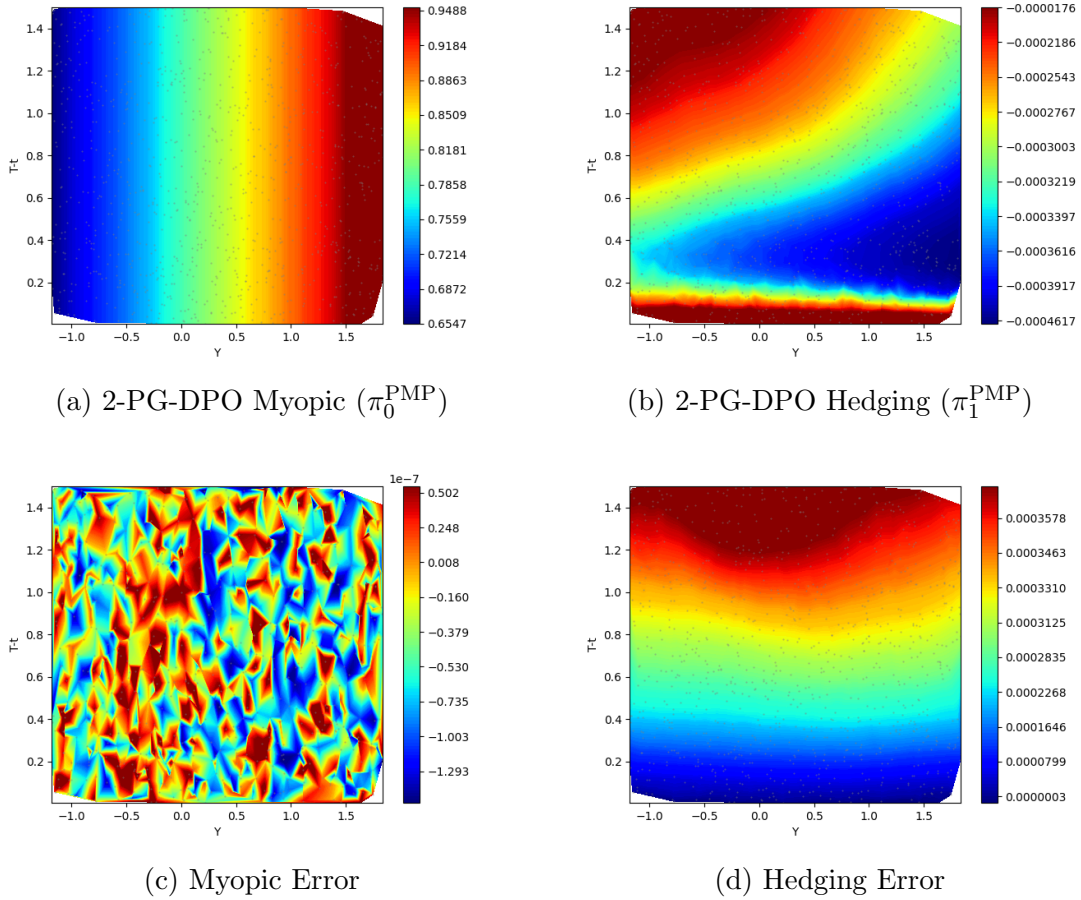


Figure 5: Decomposition of the 2-PG-DPO policy for the $n=1, k=10$ case at epoch 2000 (plotted against Y_1). Top row shows the myopic (left) and hedging (right) components. Bottom row shows their respective errors. Note the extremely small error scale for the myopic component and the very small magnitude of the hedging component itself.

state spaces. It significantly outperforms the Baseline PG-DPO approach and accurately captures the policy structure dictated by PMP, with negligible error in the myopic component and the total error determined by the precision of the hedging component estimation. This highlights the suitability of the 2-PG-DPO framework for problems involving complex, multi-factor dynamics influencing investment decisions.

4.5 High-Dimensional Performance (n=50, k=10)

Finally, we evaluate the performance in the most challenging setting considered: a high-dimensional problem with $n=50$ assets and $k=10$ state variables. This scenario fully tests the scalability and effectiveness of the proposed methods in dimensions where traditional DP methods are intractable. Similar to the previous section, the visualizations focus on the policy for the first asset ($i = 1$) as a function of time-to-maturity ($T - t$) and the first state variable (Y_1), holding other state variables (Y_2, \dots, Y_{10}) constant at their long-term means ($\theta_{Y,i}$). The results shown correspond to the state after 3,000 training epochs, representing the point where the 2-PG-DPO method achieved its minimum RMSE in Figure 1c.

The challenges of high dimensionality become starkly evident for the Baseline PG-DPO method in Figure 6. While the learned policy for the first asset (6a) shows some structure, the corresponding error (6c) is extremely large, with values ranging from approximately -1.1 to -0.7. This indicates severe inaccuracies and potentially a systematic bias in the policy learned by the Baseline method when faced with the combined complexity of 50 assets and 10 state variables. This poor performance aligns with the high and slowly converging RMSE observed in Figure 1c.

In dramatic contrast, the 2-PG-DPO method continues to provide a highly accurate solution, as shown by its policy (6b) and error (6d). The error magnitude for the 2-PG-DPO policy is approximately within ± 0.02 . While this represents a slight increase in error compared to the lower-dimensional cases (e.g., $n=1, k=10$ where the error was order 10^{-4}), it is still **orders of magnitude smaller** (roughly 50 times smaller) than the error of the Baseline PG-DPO method for this same high-dimensional problem. This underscores the robustness and practical necessity of the 2-PG-DPO approach; although perfect accuracy might be harder to achieve as dimensionality increases, it remains remarkably effective and vastly superior to the direct policy learning method. The error level visually corresponds to the minimum RMSE achieved by the 2-PG-DPO method in Figure 1c.

The component decomposition in Figure 7 confirms the patterns observed previously, even in this complex setting. The myopic component (7a) still largely dictates the policy shape, and its associated error (7c) remains negligible (order 10^{-7}), demonstrating the consistent accuracy of its estimation across all dimensions tested. The hedging component (7b) appears relatively more significant here compared to the $n=1, k=10$ case, contributing visibly to the total policy shape. Crucially, the hedging error (7d) is again visually identical to the total 2-PG-DPO error (6d), confirming that the overall accuracy is dictated by the precision of estimating the hedging demands, which becomes slightly more challenging, yet remains manageable, in higher dimensions.

In conclusion, the $n=50, k=10$ results powerfully demonstrate the capability of

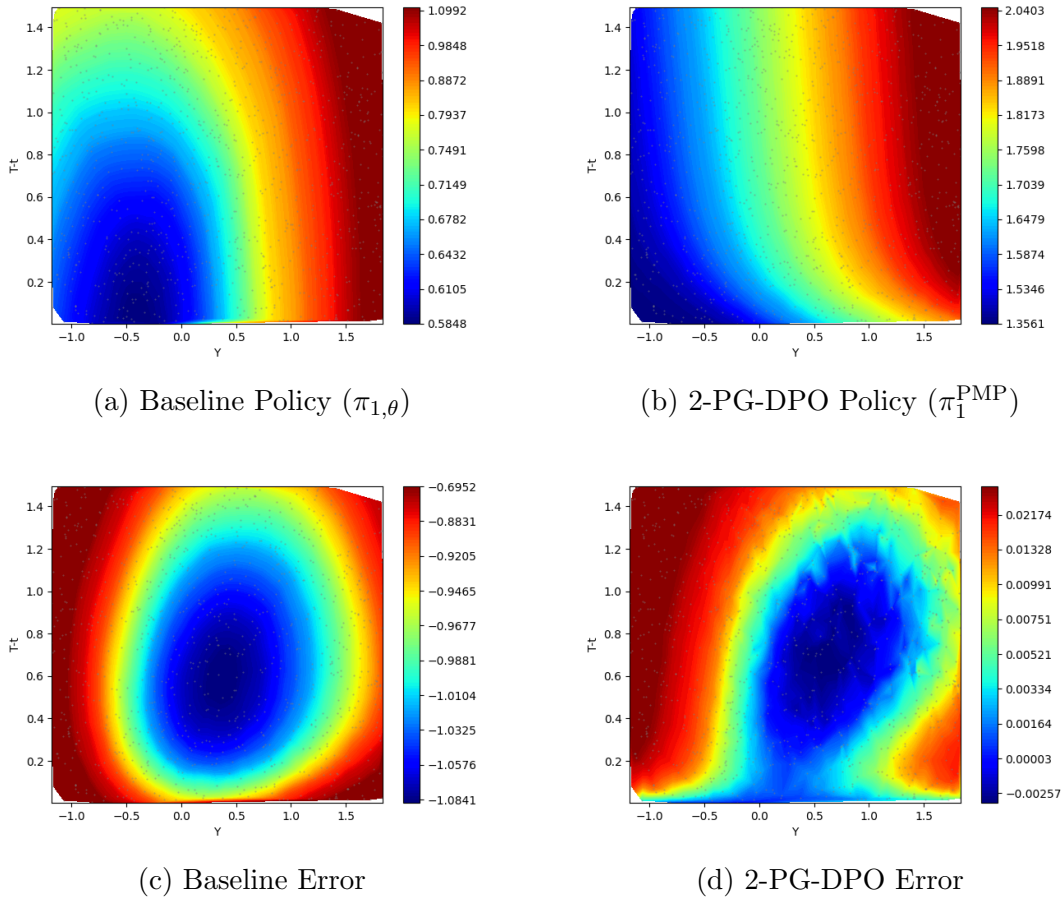


Figure 6: Comparison of total policies and errors for the first asset ($i = 1$) in the $n=50, k=10$ case at epoch 3000 (plotted against Y_1). Top row compares the policies from Baseline PG-DPO (left) and 2-PG-DPO (right). Bottom row compares their respective errors. Note the dramatic difference in error scales and magnitudes.

the 2-PG-DPO framework to “break the dimensional barrier”. While the Baseline PG-DPO struggles significantly, 2-PG-DPO delivers a highly accurate and viable solution by leveraging the structure of Pontryagin’s Maximum Principle. Despite a slight, expected increase in error compared to lower-dimensional settings, its performance remains remarkably strong and vastly superior to the baseline, solidifying its potential as a practical tool for large-scale, continuous-time portfolio optimization.

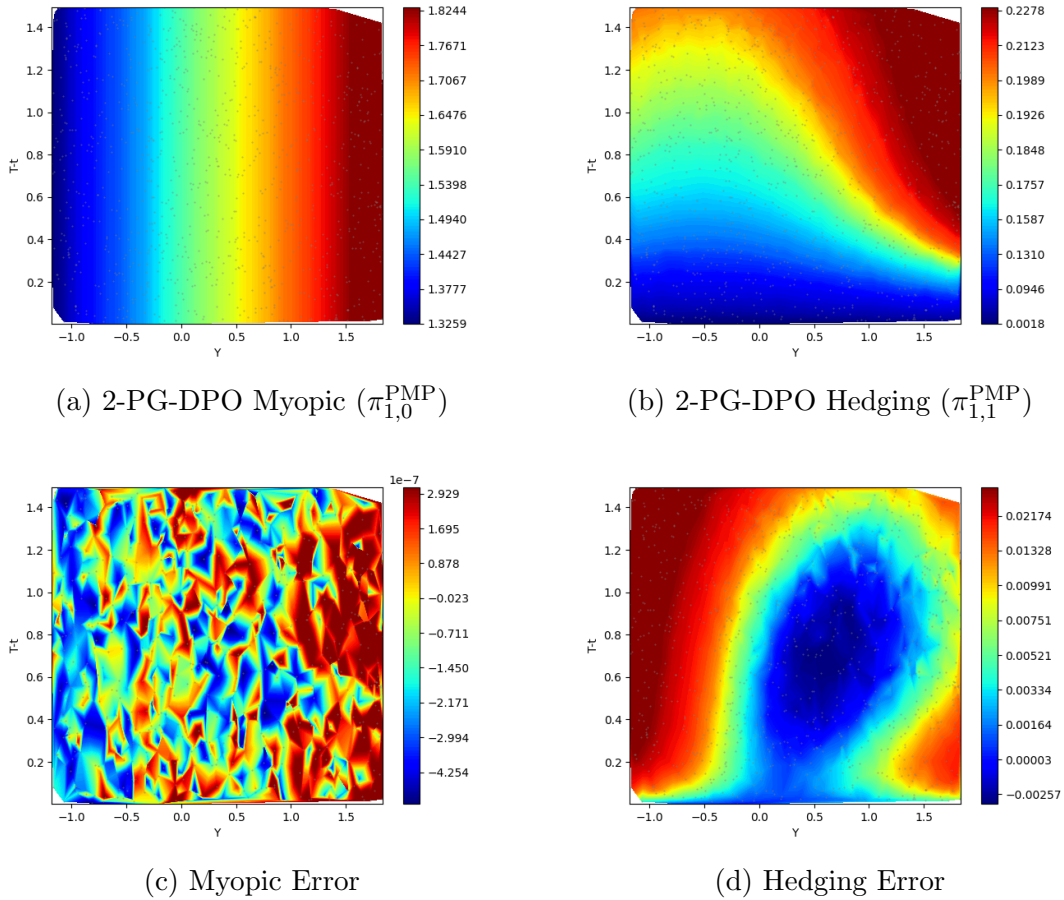


Figure 7: Decomposition of the 2-PG-DPO policy for the first asset ($i = 1$) in the $n=50, k=10$ case at epoch 3000 (plotted against Y_1). Top row shows the myopic (left) and hedging (right) components. Bottom row shows their respective errors. The myopic error remains negligible, while the hedging error dictates the total error.

5 Conclusion

In this paper, we addressed the challenge of solving high-dimensional continuous-time portfolio optimization problems, which often suffer from the “curse of dimensionality” when approached with traditional dynamic programming methods. We developed and implemented the Pontryagin-Guided Direct Policy Optimization (PG-DPO) framework, which leverages Pontryagin’s Maximum Principle (PMP) and deep learning techniques, specifically backpropagation-through-time (BPTT), to directly optimize neural network policies for investment and consumption.

A key contribution is the introduction of a highly effective “Two-Stage” PG-DPO variant. This approach utilizes a short warm-up phase to obtain stable estimates of the crucial Pontryagin costates and their derivatives via BPTT, potentially refined through Monte Carlo averaging. These estimates are then plugged directly into the analytical first-order optimality conditions derived from PMP to construct the control policy. Our numerical experiments, conducted on a multi-asset, multi-factor affine model allowing for benchmark comparisons, demonstrated that the 2-PG-DPO method significantly outperforms the baseline end-to-end approach. It achieves substantially higher accuracy and faster convergence, successfully scaling to problems with dimensions (e.g., $n=50$ assets, $k=10$ state factors) previously considered intractable for numerical HJB/PDE solvers, thereby effectively “breaking the dimensional barrier.” We specifically highlighted the method’s ability to accurately capture both myopic and complex intertemporal hedging demands by leveraging the PMP structure.

This research opens several avenues for future investigation.

Firstly, exploring the theoretical underpinnings further is crucial. While Proposition 3.1 provides heuristic support for the 2-PG-DPO approach in structured models, rigorously analyzing or establishing similar **derivative stability properties for the broader class of non-affine models** would significantly strengthen the foundation of the method. Furthermore, investigating the **theoretical convergence properties** of the PG-DPO algorithm, particularly the costate estimation process within the 2-PG-DPO variant, remains an important open question.

Secondly, extending the framework to incorporate more realistic market features is a natural next step. This includes introducing **portfolio constraints** (such as short-selling restrictions or leverage limits) and modeling **transaction costs**, which significantly alter the optimal control problem. Adapting the PG-DPO framework to handle these complexities efficiently would enhance its practical applicability. Testing the framework’s robustness and performance with **different utility functions** beyond CRRA (e.g., HARA, prospect theory) is also warranted.

Thirdly, further empirical validation and algorithmic refinements are desirable. Applying the PG-DPO framework (especially the superior 2-PG-DPO variant) to well-known **non-affine financial models** (e.g., stochastic volatility models), even in the absence of exact benchmarks, would showcase its capabilities more broadly. Conducting numerical experiments that explicitly include the optimization and evaluation of the **intermediate consumption policy**, which was omitted in the current study for benchmarking purposes, would provide a more complete assessment of the full framework. Exploring alternative **neural network architectures, optimization techniques, and variance reduction methods** could potentially lead to further performance improvements.

Finally, optimizing the implementation details, such as the warm-up duration

for the 2-PG-DPO method to balance costate accuracy against potential overfitting to simulation artifacts, deserves further attention.

Overall, the Pontryagin-Guided Direct Policy Optimization framework, particularly its Two-Stage variant, offers a promising and scalable approach for tackling complex, high-dimensional optimal control problems in continuous-time finance.

Acknowledgments

This work was supported by the National Research Foundation of Korea (NRF) grant funded by the Korea government (MSIT) (RS-2025-00562904).

References

- Balduzzi, P. & Lynch, A. W. (1999). Transaction costs and predictability: Some utility cost calculations. *Journal of Financial Economics*, 52(1), 47–78. 1
- Bellman, R. (1966). Dynamic programming. *science*, 153(3731), 34–37. 1
- Bertsekas, D. P. & Tsitsiklis, J. N. (1995). Neuro-dynamic programming: an overview. In *Proceedings of 1995 34th IEEE conference on decision and control*, volume 1 (pp. 560–564):. IEEE. 1
- Borkar, V. S. & Borkar, V. S. (2008). *Stochastic approximation: a dynamical systems viewpoint*, volume 9. Springer. 1
- Brandt, M. W., Goyal, A., Santa-Clara, P., & Stroud, J. R. (2005). A simulation approach to dynamic portfolio choice with an application to learning about return predictability. *The Review of Financial Studies*, 18(3), 831–873. 1
- Campbell, J. Y., Chan, Y. L., & Viceira, L. M. (2003). A multivariate model of strategic asset allocation. *Journal of financial economics*, 67(1), 41–80. 1
- Campbell, J. Y. & Viceira, L. M. (1999). Consumption and portfolio decisions when expected returns are time varying. *The Quarterly Journal of Economics*, 114(2), 433–495. 1
- Duarte, V., Duarte, D., & Silva, D. H. (2024). Machine learning for continuous-time finance. *The Review of Financial Studies*, 37(11), 3217–3271. 1
- Garlappi, L. & Skoulakis, G. (2010). Solving consumption and portfolio choice problems: The state variable decomposition method. *The Review of Financial Studies*, 23(9), 3346–3400. 1

- Han, J., Jentzen, A., & E, W. (2018). Solving high-dimensional partial differential equations using deep learning. *Proceedings of the National Academy of Sciences*, 115(34), 8505–8510. 1
- Huh, J. (2024). A pontryagin-guided neural policy optimization framework for merton’s portfolio problem. *arXiv preprint arXiv:2412.13101*. 1, 3, 3.1
- Karatzas, I., Lehoczky, J. P., & Shreve, S. E. (1987). Optimal portfolio and consumption decisions for a ”small investor” on a finite horizon. *SIAM journal on control and optimization*, 25(6), 1557–1586. 1
- Kim, T. S. & Omberg, E. (1996). Dynamic nonmyopic portfolio behavior. *The Review of Financial Studies*, 9(1), 141–161. 2.3.1, 3.1, B.1
- Kushner, H. J. & Yin, G. G. (2003). *Stochastic Approximation and Recursive Algorithms and Applications*. New York: Springer Science & Business Media. 1
- Liu, J. (2007). Portfolio selection in stochastic environments. *The Review of Financial Studies*, 20(1), 1–39. 3.1
- Lynch, A. W. (2001). Portfolio choice and equity characteristics: Characterizing the hedging demands induced by return predictability. *Journal of Financial Economics*, 62(1), 67–130. 1
- Merton, R. C. (1971). Optimum consumption and portfolio rules in a continuous-time model. *Journal of Economic Theory*, 3(4), 373–413. 1, 2, 3.1
- Nguwi, J. Y., Penent, G., & Privault, N. (2024). A deep branching solver for fully nonlinear partial differential equations. *Journal of Computational Physics*, 499, 112712. 1
- Pontryagin, L. S. (2014). *Ordinary Differential Equations: Adiwes International Series in Mathematics*. Elsevier. 1, 2
- Raissi, M., Perdikaris, P., & Karniadakis, G. E. (2019). Physics-informed neural networks: A deep learning framework for solving forward and inverse problems involving nonlinear partial differential equations. *Journal of Computational physics*, 378, 686–707. 1
- Yong, J. & Zhou, X. Y. (2012). *Stochastic controls: Hamiltonian systems and HJB equations*, volume 43. Springer Science & Business Media. 1, 2

A Derivation of the Adjoint Diffusion Coefficient via Itô's Lemma

In the Pontryagin framework, the adjoint (or costate) process associated with the investor's wealth X_t is identified with the partial derivative of the value function V . Concretely, we set $\lambda_t = V_X(t, X_t, \mathbf{Y}_t)$, where $\mathbf{Y}_t \in \mathbb{R}^k$ represents additional state variables and X_t is the investor's scalar wealth process. Our goal in this section is to derive the diffusion coefficient corresponding to the $d\mathbf{W}_t^X$ term in the backward SDE for λ_t , namely $\mathbf{Z}_t^{\lambda X}$ from BSDE (2), which plays a crucial role in determining the optimal portfolio via FOC (4).

Recall that under an optimal control $(\boldsymbol{\pi}_t^*, C_t^*)$, the wealth X_t^* evolves according to Eq. (1), and the k -dimensional state process \mathbf{Y}_t^* follows its own SDE, also presented in Section 2.2. The dynamics are driven by correlated Brownian motions $\mathbf{W}_t^X \in \mathbb{R}^n$ and $\mathbf{W}_t^Y \in \mathbb{R}^k$ with the joint covariance structure $\text{Cov}(d\mathbf{W}_t) = \begin{pmatrix} \Psi & \rho \\ \rho^\top & \Phi \end{pmatrix} dt$.

Since $\lambda_t = V_X(t, X_t, \mathbf{Y}_t)$, we apply Ito's multidimensional lemma to V_X . The differential $d\lambda_t$ can be expressed as:

$$\begin{aligned} d\lambda_t \text{edundant} &= V_{Xt} dt + V_{XX} dX_t + V_{X\mathbf{Y}} d\mathbf{Y}_t \\ &\quad + \frac{1}{2} V_{XXX} (dX_t)^2 + V_{XX\mathbf{Y}} (dX_t)(d\mathbf{Y}_t)^\top + \frac{1}{2} \text{Tr}(V_{X\mathbf{Y}\mathbf{Y}} (d\mathbf{Y}_t)(d\mathbf{Y}_t)^\top), \end{aligned} \tag{8}$$

where subscripts denote partial derivatives (e.g., $V_{X\mathbf{Y}}$ is the gradient w.r.t \mathbf{Y} of V_X , $V_{X\mathbf{Y}\mathbf{Y}}$ is the Hessian w.r.t \mathbf{Y} of V_X).

Our objective is to identify the coefficient of $d\mathbf{W}_t^X$ in the expansion of $d\lambda_t$. This coefficient is precisely the process $\mathbf{Z}_t^{\lambda X}$ appearing in the BSDE (2). Substituting the SDEs for dX_t and $d\mathbf{Y}_t$ (from Section 2.2) into the Ito formula (8), we observe that terms involving $d\mathbf{W}_t^X$ arise directly from the diffusion part of the $V_{XX} dX_t$ term, and indirectly from the $V_{X\mathbf{Y}} d\mathbf{Y}_t$ term due to the correlation ρ between $d\mathbf{W}_t^X$ and $d\mathbf{W}_t^Y$. A careful application of Ito's lemma, considering the quadratic variation and covariation terms related to the covariance matrix $\begin{pmatrix} \Psi & \rho \\ \rho^\top & \Phi \end{pmatrix}$, allows isolation of the full coefficient multiplying $d\mathbf{W}_t^X$. Representing $\mathbf{Z}_t^{\lambda X}$ as a $1 \times n$ row vector, this process is found to be:

$$\mathbf{Z}_t^{\lambda X} = \underbrace{(\partial_x \lambda_t^*) X_t^* \boldsymbol{\pi}_t^{*\top} \boldsymbol{\sigma}(t, \mathbf{Y}_t^*)}_{\text{Term from } V_{XX} dX_t} + \underbrace{(\partial_{\mathbf{Y}} \lambda_t^*) \boldsymbol{\sigma}_Y(t, \mathbf{Y}_t^*) \rho^\top \Psi^{-1}}_{\text{Term from } V_{X\mathbf{Y}} dY_t \text{ via correlation}}. \tag{9}$$

The first term reflects the direct impact of wealth volatility related to the portfolio choice $\boldsymbol{\pi}_t^*$, scaled by the second derivative of the value function with respect

to wealth, V_{XX} (or $\partial_x \lambda_t^*$). The second term captures the intertemporal hedging component arising from the correlation between asset returns and state variable movements, mediated by the cross-derivative of the value function V_{XY} (or $\partial_Y \lambda_t^*$).

This derivation provides the explicit form of the adjoint diffusion coefficient $\mathbf{Z}_t^{\lambda X}$, which is fundamental for understanding the structure of the optimal portfolio policy (5) and for constructing the Pontryagin adjoint equations.

B Analytic Solutions for Affine Models

This appendix provides details on the derivation of analytic solutions for the portfolio optimization problems presented in Section 2.3 under specific assumptions (no intermediate consumption, CRRA utility), typically following the Hamilton–Jacobi–Bellman (HJB) approach with an exponential-quadratic value function ansatz. We also show how these solutions connect to the Pontryagin framework.

B.1 Analytic Solution for the Multi-Asset OU Model (Section 2.3.1)

For simplicity, we assume no intermediate consumption, i.e., $C_t = 0$, and consider an investor who derives utility only from terminal wealth X_T under a CRRA objective $U(x) = \frac{x^{1-\gamma}}{1-\gamma}$. Following Kim & Omberg (1996), the associated Hamilton–Jacobi–Bellman (HJB) equation can be solved by positing a value function of the form $V(t, x, Y) = \frac{x^{1-\gamma}}{1-\gamma} \exp(g(t) + B(t)Y + \frac{1}{2}C(t)Y^2)$. Here, $g(t)$, $B(t)$, and $C(t)$ are deterministic functions of time determined by solving ordinary differential equations (ODEs) derived from the HJB equation, subject to terminal conditions $g(T) = 0$, $B(T) = 0$, and $C(T) = 0$.

From this value function, the costate $\lambda_t^* = V_x$, its derivative with respect to wealth $\partial_x \lambda_t^* = V_{xx}$, and its derivative with respect to the state $\partial_Y \lambda_t^* = V_{xY}$ have the following closed-form expressions on the optimal path (X_t^*, Y_t) :

$$\begin{aligned}\lambda_t^*(t, X_t^*, Y_t) &= (X_t^*)^{-\gamma} \exp\left(g(t) + B(t)Y_t + \frac{1}{2}C(t)Y_t^2\right), \\ \frac{\partial \lambda_t^*}{\partial x}(t, X_t^*, Y_t) &= -\gamma (X_t^*)^{-\gamma-1} \exp\left(g(t) + B(t)Y_t + \frac{1}{2}C(t)Y_t^2\right), \\ \frac{\partial \lambda_t^*}{\partial Y}(t, X_t^*, Y_t) &= (X_t^*)^{-\gamma} (B(t) + C(t)Y_t) \exp\left(g(t) + B(t)Y_t + \frac{1}{2}C(t)Y_t^2\right).\end{aligned}$$

These expressions lead to remarkably simple ratios that are central to the Pontryagin framework’s characterization of the optimal portfolio:

$$\frac{\lambda_t^*}{\partial_x \lambda_t^*} = -\frac{X_t^*}{\gamma}, \quad \frac{\partial_Y \lambda_t^*}{\partial_x \lambda_t^*} = -\frac{X_t^*}{\gamma} (B(t) + C(t)Y_t).$$

Substituting these ratios into the general Pontryagin first-order condition for the optimal portfolio $\boldsymbol{\pi}_t^*$ (which equates the marginal contribution to the Hamiltonian from investing in risky assets to zero, cf. Eq. (4) derived in Section 2.2) confirms the explicit analytic solution derived via the HJB approach:

$$\boldsymbol{\pi}^*(t, Y) = \frac{1}{\gamma} \Sigma^{-1} \left[\underbrace{(\boldsymbol{\alpha} \boldsymbol{\sigma}) Y}_{\text{Risk premium } \boldsymbol{\mu}(Y) - r\mathbf{1}} + \underbrace{\sigma_Y (\boldsymbol{\sigma} \boldsymbol{\rho}) (B(t) + C(t) Y)}_{\text{Hedging demand from } \partial_Y \lambda_t^*} \right],$$

where $\boldsymbol{\alpha} = (\alpha_1, \dots, \alpha_n)^\top$, $\boldsymbol{\rho} = (\rho_1, \dots, \rho_n)^\top$, the notation $(\boldsymbol{\alpha} \boldsymbol{\sigma})$ represents the vector $(\alpha_1 \sigma_1, \dots, \alpha_n \sigma_n)^\top$, and $(\boldsymbol{\sigma} \boldsymbol{\rho})$ represents the vector $(\sigma_1 \rho_1, \dots, \sigma_n \rho_n)^\top$. The derivation confirms that the first term captures the myopic demand driven by the instantaneous risk premium $(\boldsymbol{\mu}(Y) - r\mathbf{1}) = (\boldsymbol{\alpha} \boldsymbol{\sigma}) Y$, while the second term represents the intertemporal hedging demand, proportional to $B(t) + C(t) Y$ which arises from the state-dependency of the investment opportunity set captured by $\partial_Y \lambda_t^*$.

Substituting this $\boldsymbol{\pi}^*$ back into the HJB equation and matching coefficients in powers of Y yields the following Riccati-type ODEs for $B(t)$ and $C(t)$:

$$B(T) = 0, \quad C(T) = 0,$$

and

$$\begin{aligned} \frac{dC(t)}{dt} &= 2 \kappa_Y C(t) - \sigma_Y^2 C(t)^2 - \frac{1 - \gamma}{\gamma} \left[\beta_0 + 2 \sigma_Y C(t) \beta_1 + \sigma_Y^2 C(t)^2 \beta_2 \right], \\ \frac{dB(t)}{dt} &= \kappa_Y B(t) - \sigma_Y^2 B(t) C(t) + \frac{1 - \gamma}{\gamma} \left[\sigma_Y^2 B(t) C(t) \beta_2 + \sigma_Y B(t) \beta_1 \right] - \kappa_Y \theta_Y C(t), \end{aligned}$$

where β_0 , β_1 , and β_2 are quadratic forms involving the model parameters:

$$\beta_0 := (\boldsymbol{\alpha} \boldsymbol{\sigma})^\top \Sigma^{-1} (\boldsymbol{\alpha} \boldsymbol{\sigma}), \quad \beta_1 := (\boldsymbol{\alpha} \boldsymbol{\sigma})^\top \Sigma^{-1} (\boldsymbol{\sigma} \boldsymbol{\rho}), \quad \beta_2 := (\boldsymbol{\sigma} \boldsymbol{\rho})^\top \Sigma^{-1} (\boldsymbol{\sigma} \boldsymbol{\rho}).$$

Once $B(t)$ and $C(t)$ are obtained by backward integration from their terminal conditions, substituting them into $\boldsymbol{\pi}^*(t, Y)$ yields the closed-form optimal strategy balancing myopic and hedging demands. The function $g(t)$ can also be found by integrating another ODE involving $B(t)$ and $C(t)$, but it does not affect the optimal policy $\boldsymbol{\pi}^*$.

B.2 Analytic Solution for the Multi-Asset Multi-Factor Model (Section 2.3.2)

For simplicity, we again assume no intermediate consumption ($C_t = 0$) and focus on an investor who maximizes the expected utility of terminal wealth under CRRA

utility $U(x) = \frac{x^{1-\gamma}}{1-\gamma}$. Following related literature on multi-factor affine models, we posit a value function of the form

$$V(t, x, \mathbf{Y}) = \frac{x^{1-\gamma}}{1-\gamma} \exp\left\{g(t) + \mathbf{B}(t)^\top \mathbf{Y} + \frac{1}{2} \mathbf{Y}^\top \mathbf{C}(t) \mathbf{Y}\right\},$$

where $\mathbf{B}(t)$ is an $n \times 1$ vector, $\mathbf{C}(t)$ is an $n \times n$ symmetric matrix, and $g(t)$ is a scalar function, all satisfying ODEs derived from the HJB equation, with terminal conditions $g(T) = 0$, $\mathbf{B}(T) = \mathbf{0}$ and $\mathbf{C}(T) = \mathbf{0}$.

Define the relevant matrices and vectors:

$$\boldsymbol{\sigma} = \text{diag}(\sigma_1, \dots, \sigma_d), \quad \boldsymbol{\sigma}_Y = \text{diag}(\sigma_{Y,1}, \dots, \sigma_{Y,n}), \quad \Sigma = \boldsymbol{\sigma} \Psi \boldsymbol{\sigma},$$

where $\Psi \in \mathbb{R}^{d \times d}$ is the correlation matrix for the d risky assets, and let $\rho \in \mathbb{R}^{d \times n}$ be the cross-correlation matrix between these assets and the n -dimensional factor Brownian motion \mathbf{W}_t^Y . Also let $\mathbf{A} = (\boldsymbol{\alpha}_1, \dots, \boldsymbol{\alpha}_d)^\top \in \mathbb{R}^{d \times n}$ collect the factor loadings $\boldsymbol{\alpha}_i \in \mathbb{R}^n$ for each asset i .

The costate $\lambda_t^* = V_x$, its derivative with respect to wealth $\partial_x \lambda_t^* = V_{xx}$, and its gradient ($n \times 1$ vector) with respect to the state vector $\partial_{\mathbf{Y}} \lambda_t^* = V_{x\mathbf{Y}}$ are given by:

$$\begin{aligned} \lambda_t^*(t, X_t^*, \mathbf{Y}_t) &= (X_t^*)^{-\gamma} \exp\left(g(t) + \mathbf{B}(t)^\top \mathbf{Y}_t + \frac{1}{2} \mathbf{Y}_t^\top \mathbf{C}(t) \mathbf{Y}_t\right), \\ \frac{\partial \lambda_t^*}{\partial x}(t, X_t^*, \mathbf{Y}_t) &= -\gamma (X_t^*)^{-\gamma-1} \exp\left(g(t) + \mathbf{B}(t)^\top \mathbf{Y}_t + \frac{1}{2} \mathbf{Y}_t^\top \mathbf{C}(t) \mathbf{Y}_t\right), \\ \frac{\partial \lambda_t^*}{\partial \mathbf{Y}}(t, X_t^*, \mathbf{Y}_t) &= (X_t^*)^{-\gamma} (\mathbf{B}(t) + \mathbf{C}(t) \mathbf{Y}_t) \exp\left(g(t) + \mathbf{B}(t)^\top \mathbf{Y}_t + \frac{1}{2} \mathbf{Y}_t^\top \mathbf{C}(t) \mathbf{Y}_t\right). \end{aligned}$$

These yield the following scalar and vector ratios, which simplify the PMP optimality conditions:

$$\frac{\lambda_t^*}{\partial_x \lambda_t^*} = -\frac{X_t^*}{\gamma}, \quad \frac{\partial_{\mathbf{Y}} \lambda_t^*}{\partial_x \lambda_t^*} = -\frac{X_t^*}{\gamma} (\mathbf{B}(t) + \mathbf{C}(t) \mathbf{Y}_t).$$

Substituting these into the vector form of the PMP first-order condition for the optimal portfolio $\boldsymbol{\pi}_t^* \in \mathbb{R}^d$, (cf. Eq. (5) derived in Section 2.2):

$$\boldsymbol{\pi}_t^* = -\frac{1}{X_t^* \partial_x \lambda_t^*} \Sigma^{-1} \left\{ \lambda_t^* (\boldsymbol{\mu}(\mathbf{Y}_t) - r\mathbf{1}) + \boldsymbol{\sigma} \rho \boldsymbol{\sigma}_Y [\partial_{\mathbf{Y}} \lambda_t^*] \right\},$$

where the risk premium vector is $\boldsymbol{\mu}(\mathbf{Y}_t) - r\mathbf{1} = \boldsymbol{\sigma} \mathbf{A} \mathbf{Y}_t$, we precisely recover the analytic solution obtained from the HJB framework:

$$\boldsymbol{\pi}^*(t, \mathbf{Y}) = \frac{1}{\gamma} \Sigma^{-1} \left[\underbrace{\boldsymbol{\sigma} \mathbf{A} \mathbf{Y}}_{\text{Myopic component (related to } \boldsymbol{\mu} - r\mathbf{1})} + \underbrace{\boldsymbol{\sigma} \rho \boldsymbol{\sigma}_Y (\mathbf{B}(t) + \mathbf{C}(t) \mathbf{Y})}_{\text{Hedging component (related to } \partial_{\mathbf{Y}} \lambda_t^*)} \right].$$

Here, the first bracketed term corresponds to the *myopic* component, driven by the instantaneous expected excess returns $\boldsymbol{\sigma} \mathbf{A} \mathbf{Y}$. The second bracketed term incorporates *intertemporal hedging* demands arising from the desire to hedge against unfavorable changes in the investment opportunity set, as captured by the factor sensitivities $\mathbf{B}(t) + \mathbf{C}(t)\mathbf{Y}$ (proportional to the gradient $\partial_{\mathbf{Y}} \lambda_t^*$) and the correlations encoded in ρ , Ψ , and Φ (implicitly via the ODEs).

To determine the time-dependent coefficients $\mathbf{B}(t)$ and $\mathbf{C}(t)$, we solve the backward matrix Riccati ODE system derived from substituting the value function ansatz and optimal portfolio into the HJB equation:

$$\begin{aligned} \frac{d\mathbf{C}(t)}{dt} &= \kappa_y^\top \mathbf{C}(t) + \mathbf{C}(t)\kappa_y - \mathbf{C}(t)\boldsymbol{\sigma}_Y \Phi \boldsymbol{\sigma}_Y \mathbf{C}(t) \\ &\quad - \frac{1-\gamma}{\gamma} [(\mathbf{A}^\top \boldsymbol{\sigma})\Sigma^{-1}(\boldsymbol{\sigma}\mathbf{A}) + (\mathbf{A}^\top \boldsymbol{\sigma})\Sigma^{-1}(\boldsymbol{\sigma}\rho\boldsymbol{\sigma}_Y)\mathbf{C}(t) \\ &\quad + \mathbf{C}(t)(\boldsymbol{\sigma}_Y^\top \rho^\top \boldsymbol{\sigma})\Sigma^{-1}(\boldsymbol{\sigma}\mathbf{A}) + \mathbf{C}(t)(\boldsymbol{\sigma}_Y^\top \rho^\top \boldsymbol{\sigma})\Sigma^{-1}(\boldsymbol{\sigma}\rho\boldsymbol{\sigma}_Y)\mathbf{C}(t)], \\ \frac{d\mathbf{B}(t)}{dt} &= \left[\kappa_y^\top - \mathbf{C}(t)\boldsymbol{\sigma}_Y \Phi \boldsymbol{\sigma}_Y - \frac{1-\gamma}{\gamma} (\mathbf{C}(t)(\boldsymbol{\sigma}_Y^\top \rho^\top \boldsymbol{\sigma})\Sigma^{-1}(\boldsymbol{\sigma}\rho\boldsymbol{\sigma}_Y) + (\mathbf{A}^\top \boldsymbol{\sigma})\Sigma^{-1}(\boldsymbol{\sigma}\rho\boldsymbol{\sigma}_Y)) \right] \mathbf{B}(t) \\ &\quad - \left[\mathbf{C}(t)\kappa_y - \frac{1-\gamma}{\gamma} (\mathbf{A}^\top \boldsymbol{\sigma})\Sigma^{-1}(\boldsymbol{\sigma}\mathbf{A}) \right] \boldsymbol{\theta}_y. \end{aligned}$$

subject to the terminal conditions $\mathbf{C}(T) = \mathbf{0}$ and $\mathbf{B}(T) = \mathbf{0}$. The scalar function $g(t)$ satisfies its own ODE, which depends on $\mathbf{B}(t)$ and $\mathbf{C}(t)$, but is not needed for determining the optimal portfolio.

Solving these ODEs backward in time from T to t and then substituting the resulting $\mathbf{B}(t)$ and $\mathbf{C}(t)$ into $\boldsymbol{\pi}^*(t, \mathbf{Y})$ gives the closed-form optimal strategy, explicitly capturing both *myopic* and *intertemporal hedging* components in a multi-asset, multi-factor setting.

C Proof Sketch for Proposition 3.1

We provide a proof sketch for Proposition 3.1 focusing on the affine/quadratic structure considered by Liu (2007) (?) with CRRA utility $U(w) = w^{1-\gamma}/(1-\gamma)$ (or $\ln w$). The argument relies on the specific form of the value function and the relationship between function closeness and coefficient closeness for polynomials.

Assume the true value function V^* and an approximation \tilde{V} both share the exponential-quadratic structure on a compact domain $\mathcal{D} = [t_0, T] \times [w_{min}, w_{max}] \times \mathcal{Y}$ (where \mathcal{Y} is a compact subset of \mathbb{R}^k):

$$\begin{aligned} V^*(t, w, \mathbf{y}) &= U(w) \cdot \Phi^*(\mathbf{y}, \tau) \\ \tilde{V}(t, w, \mathbf{y}) &= U(w) \cdot \tilde{\Phi}(\mathbf{y}, \tau) \end{aligned}$$

where $\tau = T - t$ and the state-dependent part has the form (adjusting notation slightly from Liu for clarity):

$$\begin{aligned}\Phi^*(\mathbf{y}, \tau) &= \exp \left[c^*(\tau) + d^*(\tau)^\top \mathbf{y} + \frac{1}{2} \mathbf{y}^\top Q^*(\tau) \mathbf{y} \right] \\ \tilde{\Phi}(\mathbf{y}, \tau) &= \exp \left[\tilde{c}(\tau) + \tilde{d}(\tau)^\top \mathbf{y} + \frac{1}{2} \mathbf{y}^\top \tilde{Q}(\tau) \mathbf{y} \right]\end{aligned}$$

Here, c, \tilde{c} are scalars, $d, \tilde{d} \in \mathbb{R}^k$, and Q, \tilde{Q} are symmetric $k \times k$ matrices, all depending smoothly on τ and the underlying model parameters.

The condition $\sup_{\mathcal{D}} |V^* - \tilde{V}| \rightarrow 0$ implies $\sup_{\tau, \mathbf{y} \in \mathcal{Y}} |\Phi^*(\mathbf{y}, \tau) - \tilde{\Phi}(\mathbf{y}, \tau)| \rightarrow 0$, since $U(w)$ is bounded and bounded away from zero on $[w_{min}, w_{max}]$. Because Φ^* and $\tilde{\Phi}$ are positive and continuous, this uniform convergence implies uniform convergence of their logarithms:

$$\sup_{\tau, \mathbf{y} \in \mathcal{Y}} |\ln \Phi^*(\mathbf{y}, \tau) - \ln \tilde{\Phi}(\mathbf{y}, \tau)| \rightarrow 0$$

This means the quadratic polynomials in the exponents are uniformly close:

$$\sup_{\tau, \mathbf{y} \in \mathcal{Y}} |(c^* + d^{*\top} \mathbf{y} + \frac{1}{2} \mathbf{y}^\top Q^* \mathbf{y}) - (\tilde{c} + \tilde{d}^\top \mathbf{y} + \frac{1}{2} \mathbf{y}^\top \tilde{Q} \mathbf{y})| \rightarrow 0$$

It is a standard result that uniform convergence of polynomials on a compact set implies the convergence of their corresponding coefficients. Therefore, we must have uniform convergence of the coefficients with respect to $\tau \in [0, T - t_0]$:

$$\sup_{\tau} |c^*(\tau) - \tilde{c}(\tau)| \rightarrow 0, \quad \sup_{\tau} \|d^*(\tau) - \tilde{d}(\tau)\| \rightarrow 0, \quad \sup_{\tau} \|Q^*(\tau) - \tilde{Q}(\tau)\| \rightarrow 0.$$

Let $\varepsilon_c, \varepsilon_d, \varepsilon_Q$ denote these suprema, all approaching zero. Let also $\varepsilon_\Phi = \sup |\Phi^* - \tilde{\Phi}| \rightarrow 0$.

Now, consider the spatial derivatives.

- **w-derivatives:** $V_w^* = U'(w)\Phi^*$ and $\tilde{V}_w = U'(w)\tilde{\Phi}$.

$$|V_w^* - \tilde{V}_w| = |U'(w)| |\Phi^* - \tilde{\Phi}|$$

Since $|U'(w)|$ is bounded on $[w_{min}, w_{max}]$, $\sup_{\mathcal{D}} |V_w^* - \tilde{V}_w| \leq (\sup |U'|)\varepsilon_\Phi \rightarrow 0$. Similar logic applies to V_{ww} using $U''(w)$.

- **y-gradient:** $\nabla_{\mathbf{y}} V^* = U(w)\nabla_{\mathbf{y}} \Phi^*$ and $\tilde{\nabla}_{\mathbf{y}} \tilde{V} = U(w)\nabla_{\mathbf{y}} \tilde{\Phi}$. We have $\nabla_{\mathbf{y}} \Phi^* = \Phi^*(d^* + Q^* \mathbf{y})$.

$$\nabla_{\mathbf{y}} \Phi^* - \nabla_{\mathbf{y}} \tilde{\Phi} = (\Phi^* - \tilde{\Phi})(d^* + Q^* \mathbf{y}) + \tilde{\Phi}[(d^* - \tilde{d}) + (Q^* - \tilde{Q}) \mathbf{y}]$$

Taking norms and suprema over the compact domain \mathcal{D} (where \mathbf{y} , Φ^* , $\tilde{\Phi}$, d^* , Q^* are bounded):

$$\sup \|\nabla_{\mathbf{y}}\Phi^* - \nabla_{\mathbf{y}}\tilde{\Phi}\| \leq \varepsilon_{\Phi} \cdot M_1 + M_2[\varepsilon_d + \varepsilon_Q M_y] \rightarrow 0,$$

where M_1, M_2, M_y are finite bounds. Thus, $\sup_{\mathcal{D}} \|\nabla_{\mathbf{y}}V^* - \nabla_{\mathbf{y}}\tilde{V}\| \leq (\sup |U|)(\sup \|\nabla\Phi^* - \nabla\tilde{\Phi}\|) \rightarrow 0$.

- **yy-Hessian:** $\nabla_{\mathbf{y}}^2 V^* = U(w)\nabla_{\mathbf{y}}^2 \Phi^*$.

$$\nabla_{\mathbf{y}}^2 \Phi^* = \nabla_{\mathbf{y}}\Phi^*(d^* + Q^*\mathbf{y})^\top + \Phi^*Q^*$$

The difference $\nabla_{\mathbf{y}}^2 \Phi^* - \nabla_{\mathbf{y}}^2 \tilde{\Phi}$ involves terms containing $(\Phi^* - \tilde{\Phi})$, $(d^* - \tilde{d})$, and $(Q^* - \tilde{Q})$. Since these differences converge uniformly to zero and other terms are bounded, the uniform convergence $\sup_{\mathcal{D}} \|\nabla_{\mathbf{y}}^2 V^* - \nabla_{\mathbf{y}}^2 \tilde{V}\| \rightarrow 0$ follows.

- **wy-cross-derivatives:** $\nabla_{\mathbf{y}}V_w^* = U'(w)\nabla_{\mathbf{y}}\Phi^*$. Uniform convergence follows from the convergence of $\nabla_{\mathbf{y}}\Phi^*$ and boundedness of $U'(w)$.

This completes the sketch, demonstrating that uniform value closeness implies uniform derivative closeness when the specific structure is shared.